energy&fuels

pubs.acs.org/EF

Article

Studies on Reaction Products, Byproducts, and Intermediates in Thermal Steps of the Cu−Cl Thermochemical Cycle for Hydrogen Generation

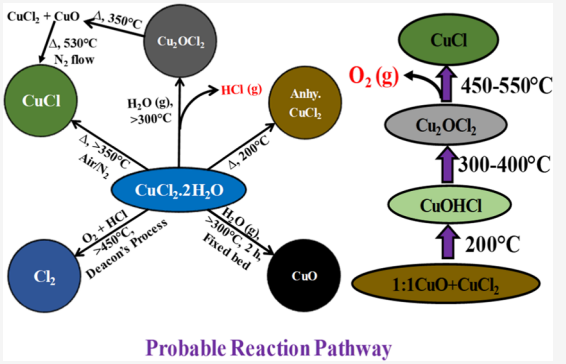
Rajendra V. Singh, Mrinal R. Pai,* Atindra M. Banerjee, Deepa Thomas, Geeta S. Patkare, Suhas Phapale, Chandrani Nayak, Vidha Bhasin, and Arvind K. Tripathi

Cite This: *Energy Fuels* 2023, 37, 15206−15221

Read Online

ACCESS | Metrics & More | Article Recommendations | Supporting Information

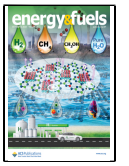
ABSTRACT: The copper−chlorine thermochemical cycle coupled with a nuclear/solar source is a potential renewable process for large-scale hydrogen production. In our earlier publications [Singh, R. V.; et al. *J. Therm. Anal. Calorim.* **2022**, *147*, 7063−7076; Singh, R. V.; et al. *Int. J. Energy Res.* **2020**, *44*(4), 2845−2863], the limitations in achieving a 100% phase-pure product, Cu_2OCl_2, in the hydrolysis step was emphasized. The present study investigated (i) the effect of the impurity phase accompanying the hydrolysis product on the kinetics of the subsequent O_2 evolution step, (ii) comparison of the thermal decomposition pathway of the hydrolysis product obtained in fixed-bed/fluidized-bed $CuCl_2$ hydrolysis with various simulated feeds using thermogravimetric mass spectrometry (TG-MS), (iii) mechanistic aspects involved in thermal decomposition of an equimolar CuO + $CuCl_2$ mixture (referred to as the substitute material, SM) from room temperature (RT) to 500 °C using *in situ* X-ray absorption spectroscopy (XAS), and (iv) the phase identification at intermediate temperatures during heating of the SM under an argon flow by *ex situ* high-temperature X-ray diffraction (HT-XRD). Main findings were that the thermal decomposition behavior of the SM was identical to the actual phase-pure hydrolysis product, Cu_2OCl_2. In the presence of the impurity phase, the decomposition temperature decreased by 30−40 °C. It was observed that moles of O_2 evolved from impure feeds are limited by *x*, where *x* corresponds to the maximum moles of Cu_2OCl_2 possible in the impure composition. Thermal decomposition of SM revealed the *in situ* formation of Cu_2OCl_2 *via* the Cu(OH)Cl phase at 300−350 °C. Further heating of Cu_2OCl_2 evolved O_2 at 450 °C as identified by MS and decomposed into single-phase CuCl at 500−550 °C. Our studies support Serban's approach [Serban, M.; et al. In *Kinetic Study of the Hydrogen and Oxygen Production Reactions in the Copper-Chlorine Thermochemical Cycle*, AIChe 2004 Spring National Meeting, April 25−29, 2004, New Orleans, LA, 2004] and conveyed that abstraction of Cl_2 by CuO may be facilitated *via* Cu_2OCl_2 formation. The *in situ* X-ray absorption near-edge structure (XANES) transformed from Cu^{2+} to Cu^{1+} with an increase in temperature. The Cu−O, Cu−Cl, and Cu−Cu bond distances and coordination number provided evidence of *in situ* formation of Cu_2OCl_2 at 300−350 °C and Cu−Cl at 500 °C. Thus, *in situ* formation of Cu_2OCl_2 from the SM has strengthened the beneficial supposition and provided the basis for considering equimolar CuO + $CuCl_2$ (SM) as a surrogate material for Cu_2OCl_2. Also, a methodology to predict the amount of O_2 evolved from impure feeds in the decomposition step is suggested.



1. INTRODUCTION

Production of clean and green hydrogen at the commercial scale is being envisaged in future.[1−5] Researchers have designed a thermochemical cycle-based route for large-scale H_2 production from water without liberating harmful emissions in the surroundings.[6,7] The cyclability of the reagents employed in the thermochemical cycle coupled with nuclear[8] or solar energy[9] sources makes it a green and renewable process. More than 200 thermochemical cycles have been devised based on Hess's law of thermodynamics.[10] Among these, iodine−sulfur (I−S),[11−14] hybrid sulfur, and copper−chlorine[15−18] thermochemical processes are found to be efficient and promising for large-scale sustainable hydrogen production. The maximum operation temperature of the Cu−Cl thermochemical cycle (T_{max} = 530 °C) is much lower as compared to sulfur-based cycles (T_{max} = 850 °C), thus offering advantages in the selection of materials of construction, and also enhances the practicability for the Cu−Cl process to be

Received: June 8, 2023
Revised: August 28, 2023
Published: September 14, 2023

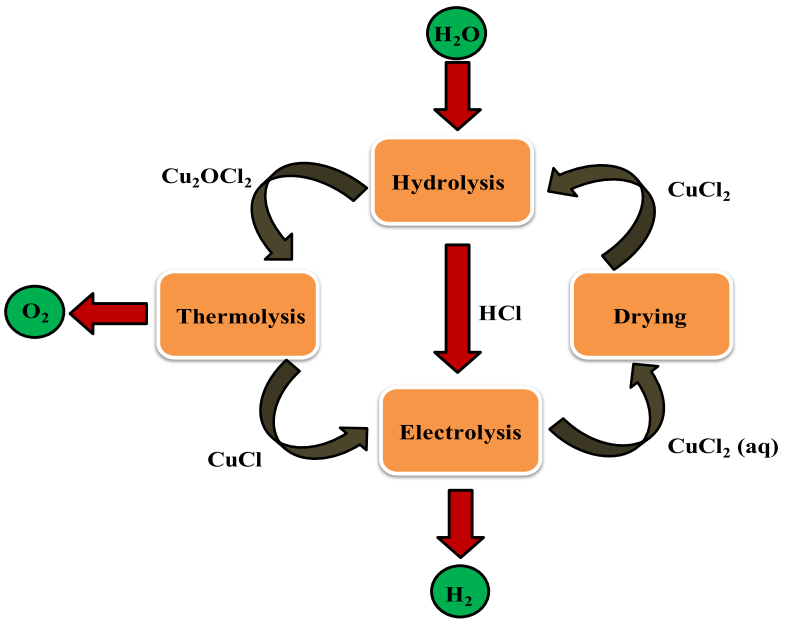


Downloaded from pubs.acs.org/enfuem/article-pdf/37/19/15206/12589762/ef3c02035.pdf by DOKUZ EYLUL UNIV user on 31 August 2026

ACS Publications

© 2023 American Chemical Society

https://doi.org/10.1021/acs.energyfuels.3c02035
Energy Fuels 2023, 37, 15206−15221



Hydrolysis Step

$$2CuCl_{2(s)} + H_2O_{(g)} \rightarrow 2HCl_{(g)} + Cu_2OCl_{2(s)} \quad 400°C,\ \Delta H = 105.2\ kJ/mol \quad (1.1)$$

Thermolysis Step

$$Cu_2OCl_{2(s)} \rightarrow 2CuCl_{(l)} + \frac{1}{2}O_{2(g)} \quad 530°C,\ \Delta H = 110.5\ kJ/mol \quad (1.2)$$

Electrolysis Step

$$2CuCl_{(l)} + 2HCl_{(l)} \rightarrow H_{2(g)} + 2CuCl_{2(l)} \quad 25°C,\ \Delta H = 18.3\ kJ/mol \quad (1.3)$$

Drying Step

$$2CuCl_{2(l)} \rightarrow 2CuCl_{2(s)} \quad T<100°C,\ \Delta H = 10.3\ kJ/mol \quad (1.4)$$

Figure 1. Schematic representation of chemical reactions involved in the four-step Cu−Cl thermochemical cycle.

coupled with a solar energy source.[18] A four-step Cu−Cl cycle has been widely accepted and studied by several institutes globally; the prominent are the Canadian Nuclear Laboratories (CNL) and University of Ontario Institute of Technology (UOIT) in Canada.[18,19] All four steps of the Cu−Cl cycle and chemical reactions involved are shown in Figure 1. In spite of the advantages, the Cu−Cl cycle encounters few challenges in each step, which needs to be addressed for efficient and economical hydrogen production. First, in the electrochemical step, copper crossover takes place across the membrane during CuCl/HCl electrolysis, which lowers the efficiency of the electrolyzer; another hindrance is incomplete recovery of the spent electrolyte from the anolyte.[19] Water as a reactant enters into the hydrolysis step of the Cu−Cl cycle followed by the decomposition step. In the hydrolysis step, the side reaction of $CuCl_2$ thermolysis to CuCl and requirement of a high steam/copper ratio are main challenges and were addressed using a fixed-bed reactor in our earlier publication.[16] Non-availability of commercial Cu_2OCl_2, its labile nature, and the presence of the impurity phase are challenges in the most energy-intensive decomposition step of the CuCl cycle.[20,21] It is important to optimize all four steps so that the overall process becomes efficient and economical.

During the hydrolysis step, $CuCl_2$ reacts with steam and produces $Cu_2OCl_2(s)$ and HCl(g) at 350−400 °C (Figure 1). Cu_2OCl_2 underwent thermal decomposition at 530 °C and yielded a green-colored solid, cuprous chloride (CuCl), along with evolution of oxygen in the subsequent decomposition step (Figure 1). Collectively, hydrolysis and decomposition are also known as thermal steps. For kinetic and mechanistic investigations on the decomposition step, the hydrolysis product (HP), Cu_2OCl_2, was required. Since it is commercially unavailable, researchers attempted to synthesize it by alternate routes. Krivovichev et al.[22] synthesized Cu_2OCl_2 by chemical transport reactions using an equimolar mixture of CuO and $CuCl_2$ at temperatures from 370 to 470 °C, while Kawashima et al.[23] prepared Cu_2OCl_2 by treating a mixture of CuO and $CuCl_2$, at 350 °C in a CO_2 atmosphere for 24 h. Nixon et al.[24] synthesized Cu_2OCl_2 by allowing the starting materials CuCl or $CuCl_2{\cdot}2H_2O$ to undergo partial oxidation in flowing dry air at 375 °C for 48 h. Widely, a 1:1 molar mixture of CuO(s) and $CuCl_2(s)$ is also accepted as a mimic of Cu_2OCl_2. However, the main aim is to prepare phase-pure Cu_2OCl_2 from water in the $CuCl_2$ hydrolysis step of the Cu−Cl process (Figure 1). Singh et al.[16] reported fixed-bed $CuCl_2$ hydrolysis to Cu_2OCl_2, and a conversion of 97% was observed at a gas hourly space

https://doi.org/10.1021/acs.energyfuels.3c02035
Energy Fuels 2023, 37, 15206−15221

Downloaded from pubs.acs.org/enfuem/article-pdf/37/19/15206/12589762/ef3c02035.pdf by DOKUZ EYLUL UNIV user on 31 August 2026

Table 1. Comparison of the Present Study with the Reported Literature Studies on Thermal Decomposition of Cu_2OCl_2

s. no	title of the study	experimental conditions	major findings	reference
1	probing temperature-dependent $CuCl_2$ hydrolysis and thermolysis reaction using *in situ* X-ray absorption spectroscopy (XAS)	*in situ* XAS and thermogravimetric analysis	mechanistic aspects of $CuCl_2$ thermolysis and hydrolysis using *in situ* XAS	Singh et al. 15
2	investigations on the hydrolysis step of the copper−chlorine thermochemical cycle for hydrogen production	fixed-bed reactor for hydrolysis reactions, TG-MS, TPD, XAS, XRD, and isothermal TG	performance evaluation of $CuCl_2$ hydrolysis on a fixed-bed reactor as a function of different parameters; effect of ball milling on reaction kinetics; rate constant and activation energy derived for the hydrolysis reaction using isothermal TG; quantification of the fixed-bed hydrolysis product using titrations, TG, TPD, and XANES; and explanation of the hydrolysis mechanism using the shrinking-core model	Singh et al. 16
3	experimental study on the mechanism and kinetics of the $CuCl_2$ hydrolysis reaction of the Cu−Cl thermochemical cycle in a fluidized-bed reactor	$CuCl_2$ hydrolysis in the fluidized-bed reactor and XRD Rietveld analysis for quantification	Cu_2OCl_2 decomposes to $CuCl_2$ and CuO depending on time, temperature, and steam concentration	Thomas et al. 25
4	mechanistic and kinetic study of the thermolysis reaction with hydrolysis step products in the Cu−Cl thermochemical cycle	thermolysis experiments with the CuO−$CuCl_2$ equimolar mixture and hydrolysis reactor product Cu_2OCl_2 and mechanistic studies using isoconversional analysis for multistep solid decomposition reactions	mechanism and kinetics of the thermolysis reaction with the CuO−$CuCl_2$ equimolar mixture and Cu_2OCl_2 (470−575 °C); similar conversion was seen in both cases, and it increased with the $CuCl_2$ fraction	Thomas et al. 21
4	hydrolysis of $CuCl_2$ in the Cu−Cl thermochemical cycle for hydrogen production: experimental studies using a spray reactor with an ultrasonic atomizer	using the ultrasonic nozzle, parameters such as nozzle power, H_2O (steam)/Cu, and preflushing conditions have been studied to follow the formation of CuCl and Cu_2OCl_2	appreciable yield of Cu_2OCl_2 was obtained at H_2O/Cu = 15 and a furnace temperature of 370 °C	Ferrandon et al. 26
5	development of the low-temperature Cu−Cl thermochemical cycle	thermolysis of the equimolar CuO and $CuCl_2$ mixture and Cu_2OCl_2 (prepared by heating (370−470 °C) stoichiometric amounts of CuO and $CuCl_2$)	O_2 yield of 85% obtained at 500 °C and CuCl with traces of $CuCl_2$ was obtained as the product of thermolysis	Lewis et al 27.
6	byproducts and reaction pathways for integration of the Cu−Cl cycle of hydrogen production	thermolysis reaction using equimolar CuO and $CuCl_2$	theoretical analysis of the decomposition of a mixture of CuO and $CuCl_2$ was also performed in this paper; decomposition of copper oxychloride is preferable over a mixture of $CuCl_2$ and CuO in the oxygen production step	Marin et al. 28
7	hybrid cycle with electrolysis using a Cu−Cl system	recirculation under He with H_2O vapor pressure maintained at 92 mmHg	the paper proposed the hybrid thermochemical and electrolysis cycle and presented preliminary results; $CuCl_2$ hydrolysis started above 300 °C and maximum O_2 evolution around 400 °C	Dokiya et al. 29
8	Sur la Formation des Chlorures Culvriques par Vola Seche. II.—Thermolyse des Chlorures Neutras et Basiques	thermogravimetric analysis done to compare the experimental results	CuO*$CuCl_2$ behaves similar to Cu_2OCl_2 during decomposition with a Gibbs energy of reaction of 61.3 and 68.7 kJ/mol and equilibrium at 530 and 610 °C, respectively	Walter-Levy and Goreaud et al. 30
9	thermochemical production of hydrogen: synthesis, characterization, and decomposition of copper oxychloride	recorded TG and gas analysis of the reaction products to investigate the Cu_2OCl_2 decomposition under a dry air and inert atmosphere.	thermal decomposition mechanism using weight loss in TG was proposed under air and argon; their study tried to explain both the observed and published data	Nixon et al. 24
10	to study effect of the impurity phase on the decomposition step of the Cu−Cl cycle	HT-XRD, TG-MS, *in situ* XAS	formation of Cu_2OCl_2 *via* Cu(OH)Cl above 300 °C and decomposition above 400 °C, almost pure CuCl at 550 °C	current work

https://doi.org/10.1021/acs.energyfuels.3c02035
Energy Fuels 2023, 37, 15206−15221

Downloaded from pubs.acs.org/enfuem/article-pdf/37/19/15206/1258976 2/ef3c02035.pdf by DOKUZ EYLUL UNIV user on 31 August 2026

Table 2. List of Samples with Nominal Compositions, Description, and Abbreviated Names

s. no	sample composition	description	sample abbreviation
1	anhy. $CuCl_2$ + CuO (1:1 molar ratio) (simulated feed sample)	mechanical mixture; it may be considered a substitute material (SM) of Cu_2OCl_2	SM
2	anhy. $CuCl_2$ + 2CuO (1:2 molar ratio) (simulated feed sample)	mechanical mixture; in this, excess of CuO is added as the impurity phase (IMP)	IMP-1
3	anhy. $CuCl_2$ + 2CuO + 0.5CuCl (1:2:0.5 molar ratio) (simulated feed sample)	mechanical mixture. In this, excess of CuO and cuprous chloride, CuCl, was added as the impurity phase (IMP)	IMP-2
4	phase-pure CuO	commercial phase-pure CuO was also investigated for oxygen evolution comparison	CuO
5	Cu_2OCl_2 actual hydrolysis product (HP)	Cu_2OCl_2 (purity ∼95%) prepared in the hydrolysis step using ball-milled $CuCl_2$ in a fixed-bed reactor	HP-Fix-1
6	Cu_2OCl_2 actual hydrolysis product (HP)	Cu_2OCl_2 (purity ≥70%) prepared in the hydrolysis step using unball-milled $CuCl_2$ in a fixed-bed reactor	HP-Fix-2
7	Cu_2OCl_2 actual hydrolysis product (HP)	Cu_2OCl_2 (purity ≥95%) prepared in the hydrolysis step using a fluidized-bed reactor	HP-Flu-1
8	Cu_2OCl_2 actual hydrolysis product (HP)	Cu_2OCl_2 (purity ≥67.7%) prepared in the hydrolysis step using a fluidized-bed reactor	HP-Flu-2

velocity (GHSV) of 17 630 h^{-1} at 400 °C using ball-milled $CuCl_2$. Thomas et al.[25] performed $CuCl_2$ hydrolysis on another type, fluidized-bed reactor and obtained a yield of 96% of Cu_2OCl_2. Ferrandon et al.[26] reported 97% yield of Cu_2OCl_2 using a spray reactor with an ultrasonic nozzle at H_2O (steam)/Cu = 15, at 370 °C. Table 1 lists various similar studies undertaken on thermal steps of the Cu−Cl thermochemical cycle.[15,16,21,24−30] Invariably, none of the reports including direct synthesis—to the best of our knowledge—have obtained a 100% phase-pure product, Cu_2OCl_2 (Table 1). We have already reported[16] the limitations in achieving the phase-pure Cu_2OCl_2 hydrolysis product. Due to its labile nature, it is easily convertible into other phases such as CuO, CuCl, and $CuCl_2$. Thus, it is very unlikely that phase-pure Cu_2OCl_2 will be obtained during the $CuCl_2$ hydrolysis step of the Cu−Cl process. The presence of an impurity phase (CuO, $CuCl_2$, or CuCl) will always (most likely) be associated with the hydrolysis product Cu_2OCl_2, and therefore, it may have adverse consequences on the kinetics of the next step, *i.e.*, decomposition step. The objective of the present study is to (i) investigate the effect of the impurity phase on the oxygen evolution step by thermogravimetric mass spectrometry (TG-MS), (ii) compare the thermal decomposition behavior of the CuO + $CuCl_2$ mixture and other simulated feeds (with the impurity phase) with the actual hydrolysis product Cu_2OCl_2 obtained in fixed-bed/fluidized-bed $CuCl_2$ hydrolysis, and (iii) investigate mechanistic insights when thermal decomposition of the equimolar CuO + $CuCl_2$ mixture takes place by recording *in situ* X-ray absorption near-edge structure (XANES) and extended X-ray absorption fine structure (EXAFS) data at the copper edge in the temperature range of room temperature (RT) to 500 °C and (iv) the phases formed at intermediate temperatures when the CuO + $CuCl_2$ mixture was heated up to 550 °C under an argon flow using *ex situ* high-temperature X-ray diffraction (HT-XRD).

For the above-mentioned investigations, evolution of oxygen and other species during decomposition of the hydrolysis product is systematically monitored by temperature-dependent TG-MS and XRD. Here, three feed mixtures, *viz.*, mechanical mixture of $CuCl_2$ + CuO (1:1 molar ratio), $CuCl_2$ + CuO (1:2 molar ratio), and $CuCl_2$ + CuO + CuCl (molar ratio 1:2:0.5 molar ratio), were prepared and investigated by subjecting these to the thermal decomposition step. Oxygen evolution yields obtained on simulated feed mixtures containing the impurity phase were compared with representative actual hydrolysis products resulted during the fixed- or fluidized-bed $CuCl_2$ hydrolysis step. The mechanistic insights of formation of the intermediate Cu_2OCl_2 and its thermal decomposition were monitored by *in situ* XAS and *ex situ* HT-XRD. These studies will also assist in strengthening the beneficial supposition that CuO + $CuCl_2$ in 1:1 molar ratio acts as a substitute material (SM) for Cu_2OCl_2, which is essential for investigative studies on the Cu−Cl cycle.

2. EXPERIMENTAL SECTION

Commercial cupric oxide (CuO), S. D. Fine Chem Limited, assay 98%, M.W. 79.55 g, cupric chloride dihydrate ($CuCl_2{\cdot}2H_2O$), S. D. Fine Chem Limited, ≥99%, M.W. 170.48 g, cuprous chloride (CuCl), Sigma-Aldrich, 97%, M.W. 99.0 g, and high-purity argon, Tripti Gases Private Ltd., Mumbai, 99.999%, were employed for the present study. $CuCl_2{\cdot}2H_2O$ was dried at 120 °C for 3 h to obtain brown-colored anhydrous $CuCl_2$. Details about $CuCl_2$ hydrolysis in fixed-bed hydrolysis are given in our earlier publication by Singh et al.[16] and fluidized-bed reactor by Thomas et al.[21,25] and in Section S1, Supporting Information. A schematic of the fixed-bed reactor is given in Figure S1 of the Supporting Information. To simulate the hydrolysis product with the impurity phase, several mechanical mixtures were prepared and subjected to TG-MS and XAS studies. The list of mechanical mixtures along with their descriptions and abbreviations is given in Table 2.

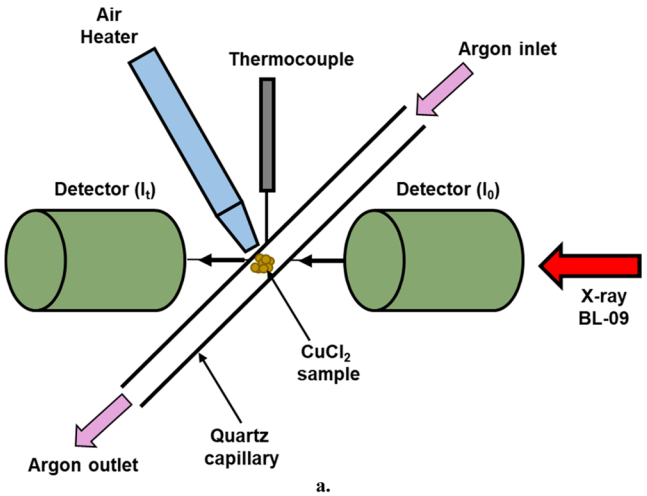
Powder XRD data were recorded in the range of 10−70° at a rate of 1°/min on a Philips diffractometer (model PW 1710), equipped with a graphite monochromator and Ni-filtered Cu Kα radiation. A Bragg−Brentano diffractometer is commonly used for geometry for diffraction. TG profiles were recorded on a LINSEIS TG-DTA instrument in the range of 35−1000 °C at a scan rate of 10 °C/min under an argon atmosphere. Simultaneously, a THERMO Star, PFEIFFER, mass spectrometer hyphenated with thermogravimetry as evolved gas analyzer (EGA), was employed to identify the constituents of the evolved gases. TG-MS was calibrated using calcium oxalate as a standard as explained in Section S2 of the Supporting Information. A typical thermogram of calcium oxalate is shown in Figure S2, and weight loss details are given in Table S1 of the Supporting Information.

In situ XAS (EXAFS and XANES) data were recorded to study the thermolysis of the SM (CuO and $CuCl_2$ in 1:1 molar ratio) mixture. The sample was heated from RT to 500 °C in a quartz capillary reactor using an air heater in a constant argon gas flow. The sample in the powdered form was loaded in a quartz capillary of 250 mm length, 3 mm outer diameter, and 0.2 mm wall thickness. It was heated from top using an air heater operating with compressed air. A thermocouple is fixed on the surface of the quartz capillary reactor to record the sample temperature. The photograph and schematic of

Downloaded from pubs.acs.org/enfuem/article-pdf/37/19/15206/12589762/ef3c02035.pdf by DOKUZ EYLUL UNIV user on 31 August 2026

https://doi.org/10.1021/acs.energyfuels.3c02035
Energy Fuels 2023, 37, 15206−15221

the experimental setup are shown in Figure 2. Time-resolved X-ray absorption spectroscopy measurements of the sample at the Cu K



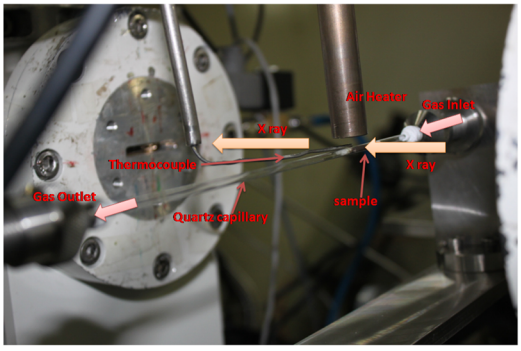


Figure 2. Schematic (a) and a photograph (b) of *in situ* XAS setup.

edge were carried out in transmission mode at the scanning EXAFS beamline (BL-9) at the Indus-2 Synchrotron Source (2.5 GeV, 100 mA) at the Raja Ramanna Centre for Advanced Technology (RRCAT), Indore, India.[31,32] For *in situ* XAS measurements in transmission mode, the quartz capillary tube reactor with a sample is placed between two ionization chamber detectors. The first ionization chamber measures the incident flux (I_0), and the second ionization chamber measures the transmitted intensity (I_t), and the absorbance of the sample is obtained as $\mu = \log(-I_t/I_0)$.

3. RESULTS

3.1. Quantification of the Hydrolysis Product Copper Oxychloride, Cu_2OCl_2. As shown in the schematic of the Cu−Cl cycle (Figure 1), the hydrolysis of $CuCl_2$ is one of the most important and crucial steps of the Cu−Cl cycle. In our earlier reports, we have performed this reaction using an indigenously developed fixed-bed reactor,[16] and our collaborators have performed it in a fluidized-bed reactor.[25] In the fixed-bed reactor, 95% yield of product, Cu_2OCl_2 (HP-Fix-1, Table 2), was achieved in our studies on hydrolysis of 0.3 g of ball-milled $CuCl_2$ at 400 °C, 17 630 h^{-1} GHSV, and S/Cu of 33.[16] Fluidized $CuCl_2$ hydrolysis resulted in more than 95% conversion to the product at 300 °C using a steam mole fraction of 0.4 in 30 min.[25] The formation of the product, Cu_2OCl_2, was always associated with production of HCl (as per eq 1.1 in Figure 1), which was trapped in an alkali trap. The amount of Cu_2OCl_2 formed was estimated using acid−base back titration of the alkali trap. Since $CuCl_2$ hydrolysis is also accompanied with some side reactions or hydrolysis beyond optimum time period yields CuO and HCl, in this case, titration results are erroneous. To confirm the yield of Cu_2OCl_2, another important methodology was devised based on oxygen evolution and adopted by most of the researchers. It is preferred over acid−base chemical titrations in which HCl formed during hydrolysis is back-titrated with the base. The possibility of error in chemical titrations arises due to the formation of HCl from reactions other than hydrolysis. Thus, oxygen evolution, which is specifically arising from decomposition of Cu_2OCl_2 in the temperature range of 450−530 °C, is more accurate for this reaction. Here, the yield of Cu_2OCl_2 was estimated as per the following eq 1

$$Cu_2OCl_2 \rightarrow 2CuCl + 0.5O_2, \quad T = 400-530^{\circ}C \tag{1}$$

Based on eq 1, the product sample was allowed to undergo decomposition under an inert atmosphere; it decomposes and liberates a stoichiometric amount of O_2 and CuCl. The O_2 evolved was monitored and quantified using thermogravimetry and confirmed by hyphenated MS. The yield of Cu_2OCl_2 obtained on fixed-bed hydrolysis was confirmed by both the titrations and O_2 evolution method and also by XAS.[16] Figure 3 shows the TG coupled with MS of HP-Fix and HP-Flu. The thermogram (TG) of both HP-Fix and HP-Flu typically shows four weight loss steps: (a) weight loss due to the adsorbed water in the temperature range of 100−200 °C, followed by (b) weight loss due to O_2 evolution, onsets at ∼400 °C and continues till 530 °C, and (c) sublimation of CuCl(s) to CuCl(g) in the range of 500−800 °C. This step partly overlaps with the O_2 evolution step. (d) Finally, reduction of CuO to Cu_2O accompanied with O_2 evolution at $T \geq 900$ °C. Formation of CuCl is expected as per eq 1 during oxygen evolution, and also, there may be some contribution by thermolysis of Cu_2OCl_2 as per reactions mentioned in eqs 2 and 3.

$$Cu_2OCl_2 \rightarrow CuCl_2 + CuO, \quad T \geq 400^{\circ}C \tag{2}$$

$$CuCl_2 \rightarrow CuCl + Cl_2, \quad T \geq 400^{\circ}C \tag{3}$$

The oxychloride Cu_2OCl_2 is quite labile in nature and on thermal treatment decomposes to CuO and $CuCl_2$ as represented by eqs 2 and 3, respectively. This also explains how CuO is formed and results in an additional oxygen evolution step at high temperature above 900 °C. The observed weight loss of all four steps is compared with theoretical or expected values in Table 3. It is clear that quantification of oxygen evolved in the second step has yielded 95 and 97 wt % Cu_2OCl_2 for both HP-Fix and HP-Flu products, respectively. The hydrolysis reactions which resulted in lower yields have given the corresponding amount of oxygen and matched with titrations.[16] Thus, oxygen evolution methodology appears to be reliable and also is useful in confirming the phase purity of hydrolysis products. MS data shown in Figure 3 for HP-Flu clearly provide evidence of evolution of water molecules at m/e = 18 at a temperature of 150−250 °C, overlapping with the first weight loss step in the range of 120−270 °C with T_{max} at 228 °C (Table 3). Similarly, emergence of the peak at a m/e of 32 in the temperature range of 400−500 °C with T_{max} at ∼450 °C signified evolution of molecular oxygen corresponding to weight loss in step 2. Both these steps also witnessed with simultaneous emergence of atomic oxygen (m/e = 16) at 228 °C due to evolved water molecules and at ∼450 °C due to oxygen gas evolution. m/e at

Downloaded from pubs.acs.org/enfuem/article-pdf/37/19/15206/12589762/ef3c02035.pdf by DOKUZ EYLUL UNIV user on 31 August 2026

https://doi.org/10.1021/acs.energyfuels.3c02035
Energy Fuels 2023, 37, 15206−15221

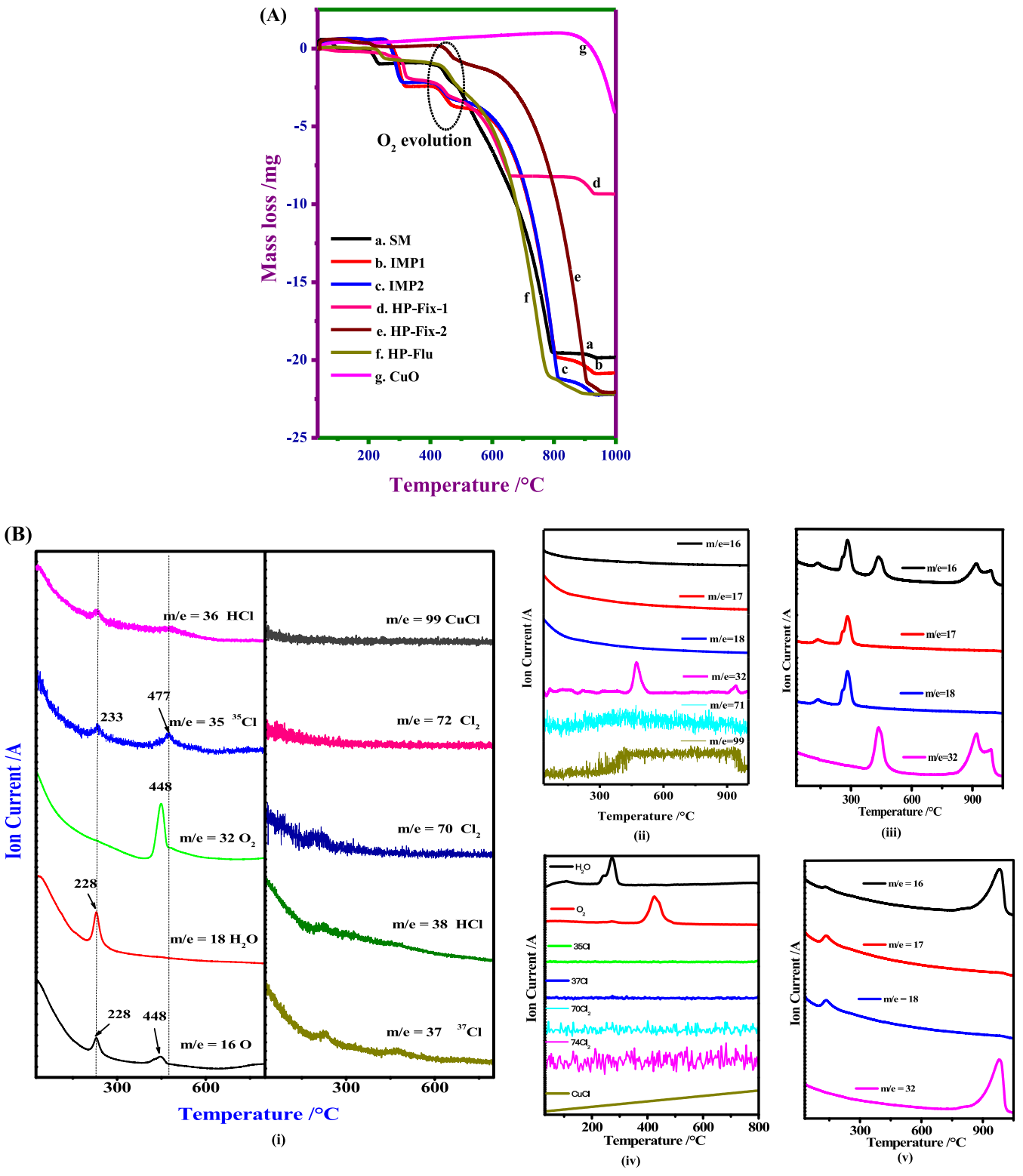


Figure 3. (A) Thermograms (TG) of different samples recorded under an argon flow in the temperature range of Rt−1000° and (B) MS spectrum of gases evolved from hyphenated TG (i) HP-Flu, (ii) SM, (iii) IMP-1, (iv) IMP-2, and (v) CuO.

35 and 37 corresponding to two isotopes of atomic Cl and m/e = 70, 72, and 74 due to molecular chlorine molecules with combination of different chlorine isotopes ($Cl^{35}Cl^{35}$, $Cl^{35}Cl^{37}$, and $Cl^{37}Cl^{37}$) were monitored to observe Cl_2 evolution. No clear evidence of Cl_2 evolution was observed. Weak signatures were observed for atomic Cl (m/e = 35, 37) at 228 and 477 °C in HP-Flu, while these were not supported by molecular Cl_2 mass spectra. Signatures of CuCl were not observed at the corresponding m/e of 99 due to the limitation of the instrument.

3.2. Effect of Impurities on the O_2 Evolution Step. Our earlier work on a fixed-bed reactor and other studies on a fluidized-bed reactor and spray reactor all have shown more than 90% conversion to Cu_2OCl_2, but none has exhibited

https://doi.org/10.1021/acs.energyfuels.3c02035
Energy Fuels 2023, 37, 15206−15221

Downloaded from pubs.acs.org/enfuem/article-pdf/37/19/15206/12589762/ef3c02035.pdf by DOKUZ EYLUL UNIV user on 31 August 2026

Table 3. Weight Loss and Species Evolved in Different Steps of Thermogram Recorded for Simulated Mixtures and Actual $CuCl_2$ Hydrolysis Products Obtained in Fixed-Bed and Fluidized-Bed Reactor Setups

sample	details	step 1	step 2	step 3	step 4
SM	T (°C)	190−235	430−510 with T_{max} = 450 from TG	500−800	940
	observed mass change (%)	−3.64(x = 0.7)	−7.24	−78.23[a]	−10.0
	theoretical mass change (%)	−10.5(x = 2)	−7.47		10.05
	species evolved-MS	H_2O	O_2		O_2
IMP-1	T (°C)	200−300	390−470 with T_{max} = 435 from TG	500−780	
	observed mass change (%)	−8.72(x = 1.62)	−5.04	−42.56[a]	
	theoretical mass change (%) wrt 1:1 $CuCl_2$ + CuO	−10.7(x = 2)	−5.3		
	species evolved-MS	H_2O	O_2		O_2
IMP-2	T (°C)	200−300	399−470 with T_{max} = 435 from TG	480−800	
	observed mass change (%)	−8.97(x = 1.72)	−4.32	−47.92[a]	
	theoretical mass change (%) wrt 1$CuCl_2$ + 1CuO	−10.4(x = 2)	−4.65		
	species evolved-MS	H_2O	O_2		
HP-Fix	1 T (°C)	100−330	360−500	540−670	865−935
	observed mass change (%)	−9.5	−7.07	−23.0[a]	−5.2
	theoretical mass change (%)		−7.47		
	species evolved-MS	H_2O	O_2		O_2
	2 T (°C)	100−300	420−550	550−900	874−960
	observed mass change (%)	−1.49	−4.0	−61.7[a]	−3.0
	theoretical mass change (%)		−7.47		
HP-Flu	T (°C)	120−270	400−530	560−790	
	observed mass change (%)	−0.90	−7.15	−20.0[a]	
	theoretical mass change (%)		−7.47		
	species evolved-MS	H_2O	O_2		O_2
inferences from MS		loss of water	O_2 evolution	CuCl evaporation	O_2 evolution
CuO	less than 1% weight loss up to 800 °C with evolution of O_2 at higher temperature due to conversion of CuO to Cu_2O				

[a]Step 3 is attributed to evaporation of CuCl, and it overlaps to some extent with step 2. Moreover, it is difficult to calculate the exact amount of CuCl formed. Thus, theoretical weight loss of step 3 is not calculated.

100% phase-pure Cu_2OCl_2.[16,25,26] Due to the inherent instability of Cu_2OCl_2, it tends to decompose in other phases such as CuO, $CuCl_2$, or CuCl on exposure to heat. Thus, the product of $CuCl_2$ hydrolysis is mostly accompanied with the impurity phases CuO, CuCl, and $CuCl_2$. To investigate the effect of the impurity phase on the kinetics of O_2 evolution (next step), it is a very important aspect for the closed-loop integration of the Cu−Cl cycle. For this purpose, several feed compositions with different impurity phases were simulated, prepared, and subjected to TG-MS, and their profiles were compared with pure Cu_2OCl_2. Descriptions of these simulated feed compositions are listed in Table 2. These feed compositions are prepared by drying and grinding the commercial components CuO, anhydrous $CuCl_2$, and CuCl, followed by mixing these mechanically in appropriate stoichiometry. The XRD patterns of the initial compounds (dihydrate $CuCl_2$, anhy. $CuCl_2$, and CuO) used in the mechanical mixture are shown in Figure S3 of the Supporting Information. Among these mechanical mixtures of $CuCl_2$ + CuO, 1:1 molar ratio referred to as the SM may be considered the substitute material to pure-phase Cu_2OCl_2. Other feeds, Imp-1 ($CuCl_2$ + 2CuO) and Imp-2 (anhy. $CuCl_2$ + 2CuO + 0.5CuCl), have impurities of CuO and CuCl phases, respectively (Table 2). In addition, pure commercial CuO was also studied for comparison. TG-MS of these mixtures was carried out under an argon atmosphere (20 ml/min) in the temperature range of RT−1000 °C (10 °C/min) as shown in Figure 3. The information derived regarding observed and expected weight loss, the temperature range of each weight loss step, and identification of the evolved species in each step from MS are listed in Table 3.

Main highlights of the TG-MS studies are as follows: (i) All samples SM, Imp-1, Imp-2, and Imp-3 have shown weight loss in four steps as described above for the actual hydrolysis products, HP-Fix and HP-Flu. Thus, the patterns of weight loss and the temperature range of the simulated feeds were similar to the actual hydrolysis products, except pure CuO and (ii) pure commercial CuO, which have not shown oxygen evolution in the temperature range of 400−530 °C. It has shown only one weight loss peak at temperature ≥900 °C attributed to evolution of O_2 due to reduction of CuO to Cu_2O as shown in eq 4

$$2CuO \rightarrow Cu_2O + 0.5O_2 \uparrow, \quad T = 800-900^{\circ}C \tag{4}$$

(iii) For the SM sample, the weight loss due to O_2 evolution in step 2 of Figure 3A was quantified and it agreed with the expected values as listed in Table 3. The O_2 evolution from SM corresponds to ∼97% Cu_2OCl_2. Thus, a mechanical mixture of CuO + $CuCl_2$ in 1:1 molar ratio yields the same amount of O_2 as the pure phase of Cu_2OCl_2. (iv) For samples Imp-1 and 2, where impurity phases exist, O_2 evolution in the temperature range of 400−530 °C was quantified and compared with the expected values as listed in Table 3. In the case of additional impurities, the amount of O_2 evolved was less than expected. The decomposition temperature also decreased by 30−40 °C in the presence of CuO and CuCl impurities. However, the amount of O_2 evolved from Imp-1 and Imp-2 samples matched with the composition at which 1:1 stoichiometry of CuO and $CuCl_2$ is reached in these samples. For instance, in sample

Downloaded from pubs.acs.org/enfuem/article-pdf/37/19/15206/12589762/ef3c02035.pdf by DOKUZ EYLUL UNIV user on 31 August 2026

https://doi.org/10.1021/acs.energyfuels.3c02035
Energy Fuels 2023, 37, 15206−15221

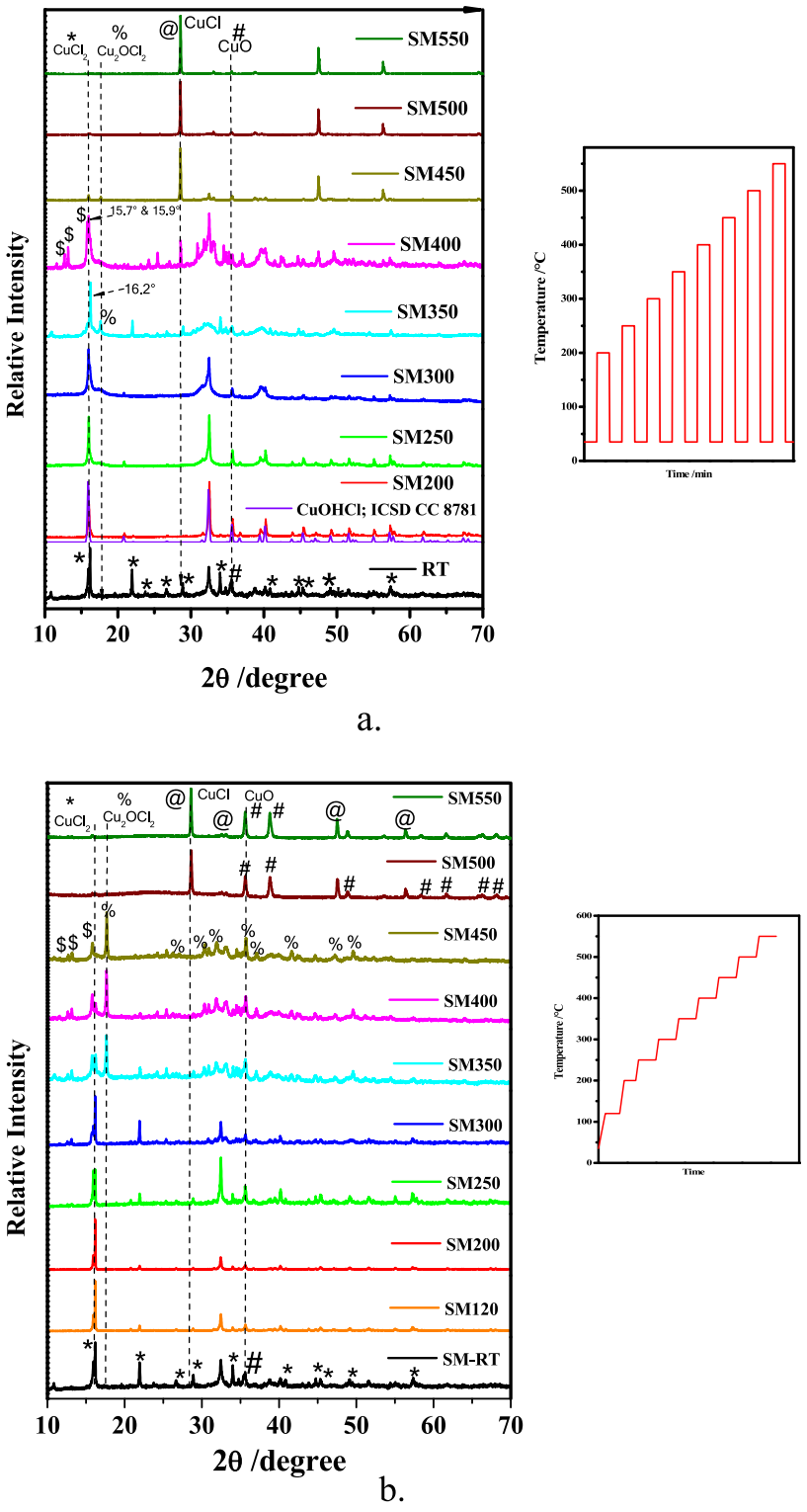


Figure 4. *Ex situ* HT-XRD patterns at intermediate temperatures for identification of phases formed when SM was subjected to two different thermal treatments under an argon flow from RT to 550 °C. (a) Repeated heating mode followed by the cooling cycle at intermediate temperatures and (b) continuous heating without the cooling cycle. A schematic representing the temperature programming ramp employed in thermal treatments is also shown. *$CuCl_2{\cdot}2H_2O$ (JCPDS# 33-0451); %Cu_2OCl_2 70-0446; @CuCl 06-0344; and #CuO 80-1917 Cu(OH)Cl ICSD # 8781.

Imp-1, the O_2 evolved was 5.04% and is explained by eqs 5 and 6. It is close to the theoretical value of 5.3% as calculated using eq 6 (Table 3). This expected value of 5.3% for O_2 evolution is obtained by considering the composition at which 1:1 stoichiometry of CuO and $CuCl_2$ for the initial weight of the sample and neglecting the excess CuO. In other words, it was observed in the present study that moles of O_2 evolved from impure samples is limited by x, where x is the maximum moles of Cu_2OCl_2 possible in the impure composition. Similarly, weight loss due to O_2 evolution in Imp-2 is explained by eqs 7 and 8. The observed weight loss of 4.32% in Imp-2 is quite in agreement with the theoretical weight loss of 4.65% (eq 8).

https://doi.org/10.1021/acs.energyfuels.3c02035
Energy Fuels 2023, 37, 15206−15221

Downloaded from pubs.acs.org/enfuem/article-pdf/37/19/15206/12589762/ef3c02035.pdf by DOKUZ EYLUL UNIV user on 31 August 2026

For Imp-1

$$2CuO + CuCl_2 \rightarrow \mathbf{Cu_2OCl_2} + CuO \quad (5)$$

$$\mathbf{Cu_2OCl_2} + CuO \rightarrow 0.5O_2 + 2CuCl + CuO \quad (6)$$

For Imp-2

$$CuCl_2 + 2CuO + 0.5CuCl \rightarrow \mathbf{Cu_2OCl_2} + CuO + 0.5CuCl \quad (7)$$

$$\mathbf{Cu_2OCl_2} + CuO + 0.5CuCl \rightarrow 0.5O_2 + CuO + 2.5CuCl \quad (8)$$

The above-mentioned results suggest that O_2 evolution matched with the maximum moles of Cu_2OCl_2 possible as explained by reactions in eqs 5 and 7. These calculations suggest that excess of CuO in Imp-1 and excess of CuO and 0.5CuCl in Imp-2 do not contribute in O_2 evolution.

All species evolved corresponding to the above-mentioned steps have been confirmed using mass spectrometric data (Figure 3). The species identified by MS were (i) m/e of 18, due to loss of water molecules and (ii) m/e of 32 corresponding to evolution of O_2 observed for step ii and iv; (iii) m/e values of 35, 37, 70, and 74 were monitored for isotopes of atomic and molecular chlorine, corresponding to ^{35}Cl, ^{37}Cl, $^{35}Cl_2$, and $^{37}Cl_2$, respectively, but no clear signals of Cl_2 evolution were observed. MS of pure CuO (Figure 3B) did not show any oxygen peak in the temperature range of 400−530 °C, while a strong O_2 peak (32) was observed at T = 930 °C. This confirms that O_2 evolution in the range of 400−530 °C is solely due to decomposition of *in situ* formed Cu_2OCl_2 phase and not due to the CuO phase present in the impurity mixtures. Pure CuO was found to be stable up to 900 °C. Evolved gas analysis from SM using MS has confirmed evolution of O_2 at 400−530 °C followed by CuCl evaporation in the range of 500−1000 °C with a poor signal/noise ratio in the MS curve. Impurity samples with excess of CuO does not show enhanced O_2 evolution at lower temperature (400 °C), Thus confirming that free CuO does not contribute in O_2 evolution at low temperature.

A mechanism of thermal transformation for actual hydrolysis products, HP-Fix (Cu_2OCl_2), under an inert atmosphere was studied in detail.[16] Here, in the present study, a similar pathway is proposed for thermal decomposition of simulated feeds (SM, Imp-1, and Imp-2) based on their TG plots. Thus, from the above-mentioned TG-MS studies, it can be inferred that Cu_2OCl_2 is an intermediate, which is formed when $CuCl_2$ + CuO (1:1 molar ratio) is heated under an inert atmosphere at 350−450 °C. Also, Cu_2OCl_2 formed further decomposes at $T \geq 500$ °C to form CuCl and O_2. Based on these studies, the amount of the oxygen that will be evolved from impure hydrolysis product samples can be predicted and will be useful for closed-loop operation of the Cu−Cl process.

$$CuCl_2{\cdot}2H_2O(s) + CuO(s) \rightarrow CuCl_2(s) + CuO(s) + 2H_2O\uparrow, \quad T = 100-200^\circ C \quad (9)$$

$$CuCl_2(s) + CuO(s) \rightarrow Cu_2OCl_2(s), \quad T = \sim 350^\circ C \quad (10)$$

$$Cu_2OCl_2(s) \rightarrow 0.5O_2\uparrow + 2CuCl(s), \quad T = 400-500^\circ C \quad (11)$$

$$CuCl(s) \rightarrow CuCl\uparrow, \quad T = 500-700^\circ C \quad (12)$$

$$2CuO(s) \rightarrow Cu_2O(s) + 0.5O_2\uparrow, \quad T = 930^\circ C \quad (13)$$

Similarity in the oxygen evolution behavior of equimolar CuO + $CuCl_2$ and Cu_2OCl_2 can be explained by assuming that *in situ* formation of Cu_2OCl_2 takes place while heating the equimolar mixture of $CuCl_2$ and CuO. To establish this hypothesis, the thermal behavior of SM was investigated by *ex situ* XRD and by recording *in situ* XAS.

3.3. *Ex Situ* High-Temperature XRD Studies on the Mixture Sample (SM). To investigate and identify the various intermediates formed during thermal decomposition of SM, it was subjected to heat treatment from RT to 550 °C under an argon flow by following two different methodologies and the sample was withdrawn intermittently at different temperatures for phase identification.

3.3.1. Intermittent Heating Followed by the Cooling Cycle at Each Temperature. The sample was kept in a quartz boat and heated in a tubular furnace under an argon flow at different temperatures, *viz.*, RT, 200 °C, 250 °C, 300 °C, 350 °C, 400 °C, 450 °C, 500 °C, and 550 °C. At each temperature, the fresh sample SM was taken and heated @10°/min and held for 10 min. This was followed by cooling of the sample. To study the phase evolution, after cooling at every temperature, the whole sample was ground and mixed and a small portion of it was subjected to powder XRD analysis (Figure 4). XRD patterns of intermediates obtained at intermittent temperature along with the schematic of the temperature programming ramp are shown in Figure 4a. The XRD pattern of SM at room temperature shows the presence of both phases as expected: $CuCl_2{\cdot}2H_2O$ (marked with *, JCPDS: 33-0451) and CuO phases (marked with #, JCPDS: 80-1917). In addition, a strong peak at 32.45° is also present, which belongs to the Cu(OH)Cl phase (ICSD# 8781). This peak also overlaps with the CuO phase but with lower intensity (72%), thus indicating the presence of the impurity phase of Cu(OH)Cl at RT. With rise in temperature to 200−250 °C, the intensity of 32.5° further increases along with a marginal shift of hkl_{100} of 16.2° toward lower 2θ values of 15.9°. At 200 and 250 °C, the pattern no longer matches with either $CuCl_2$ or CuO; instead, all peaks match completely with the Cu(OH)Cl phase as shown by overlapping the observed pattern with the reported Cu(OH)Cl pattern (ICSD Coll # 8781). Thus, $CuCl_2$ and CuO react together to form the Cu(OH)Cl phase along with loss of a water molecule as per eq 14. As mentioned in the Section 2, the simulated mixtures were prepared and then heated at 100 °C to remove the moisture, so during that also, some Cu(OH)Cl phase might have formed as indicated by the XRD pattern recorded at RT, in which the presence of the Cu(OH)Cl phase is also revealed. At 300 °C, a peak appeared at 2θ = 17.6°, which further intensified at a higher temperature of 350 °C. This peak marked by % in Figure 4a belongs to the orthorhombic Cu_2OCl_2 phase (JCPDS: 70-0446). Thus, formation of Cu_2OCl_2 from CuO + $CuCl_2$ *via* Cu(OH)Cl is indicated. Based on these inferences, eqs 9 and 10 can be modified as the following eqs 14 and 15

$$CuCl_2{\cdot}2H_2O(s) + CuO(s) \rightarrow 2Cu(OH)Cl(s) + H_2O\uparrow, \quad T = 100-250^\circ C \quad (14)$$

Downloaded from pubs.acs.org/enfuem/article-pdf/37/19/15206/12589762/ef3c02035.pdf by DOKUZ EYLUL UNIV user on 31 August 2026

https://doi.org/10.1021/acs.energyfuels.3c02035
Energy Fuels 2023, 37, 15206−15221

$$2Cu(OH)Cl(s) \rightarrow Cu_2OCl_2(s) + H_2O \uparrow ,$$
$$T = 300-350^{\circ}C \quad (15)$$

The peak corresponding to the Cu_2OCl_2 phase at $2\theta = 17.6^{\circ}$ increases in intensity up to 350 °C temperature. Thus, *in situ* formation of Cu_2OCl_2 was observed with an onset temperature of 300 °C, further increased at 350 °C, and continued up to 400 °C. At 400 °C, the intensity of the Cu_2OCl_2 phase declined; main peaks reappeared at 15.7, 15.9, and 32.5° along with emergence of few weak peaks at lower angles of 12.7 and 13.2°. Collectively, the whole XRD pattern at 400 °C cannot be attributed to one particular phase. On closer scrutiny, we found that at 400°, the peak at 16.2° due to $CuCl_2$ completely vanished and instead was replaced by a doublet at 15.7 and 15.9°. On extensive search for possible phase which gives rise to low angle peaks, it was found that copper aqua chlorates and copper chloride hydrates show peaks in the range of 12−14°. Finally, the XRD pattern at 400 °C was resolved. The peaks at lower angles along with almost 100% peak at 15.7° closely matched with formation of copper chloride hydroxide hydrate $Cu_3Cl_4(OH)_2{\cdot}2H_2O$ (marked by $, JCPDS# 24-0353). Probably, it is accompanied with the Cu(OH)Cl phase as indicated by the prominent 32.5° peak. Thus, the pattern at 400 °C is probably a transition from Cu_2OCl_2 to CuCl *via* the $Cu_3Cl_4(OH)_2{\cdot}2H_2O$ phase. Since the XRD patterns are recorded after cooling, it is quite likely that Cu_2OCl_2 on cooling absorbed water molecules and converted into the $Cu_3Cl_4(OH)_2{\cdot}2H_2O$ phase as revealed by XRD analysis. The intensity of Cu_2OCl_2, $CuCl_2$, or Cu(OH)Cl or any other oxy hydrate phase completely diminished and transformed into the CuCl phase at 450 °C and completely disappeared at 500 °C. The CuCl phase with the most intense peak at 2θ = 28.5° (marked as @ JCPDS card no. 06-0344) started appearing with appreciable intensity at 400 °C, confirming simultaneous decomposition of Cu_2OCl_2 into CuCl as per eq 1. The single phase CuCl appeared at 550 °C.

3.3.2. Continuous Heating without Cooling. Here, an equimolar mixture of CuO and $CuCl_2$, SM, was subjected to continuous heat treatment from RT to 550 °C under an argon flow @10°/min and held for 5 min at temperatures with an increase of 50 °C. During temperature hold, a small amount of powder sample was withdrawn and was analyzed by XRD. After sampling, the heating of SM was continued as per the temperature programming ramp shown in Figure 4b. Here, mainly, cooling of the sample at every temperature is avoided and the sample SM is continuously heated up to 550 °C. XRD patterns at different temperatures are shown in Figure 4b. Here, few differences were observed in the phases identified particularly in the range of 300−450 °C. The RT pattern is identical as mentioned above with the CuO + $CuCl_2{\cdot}2H_2O$ phase along with some Cu(OH)Cl phase. At 120, 200, and 250 °C, existence of the single phase Cu(OH)Cl was observed, which intensified with temperature up to 250 °C. At 300 °C, the Cu(OH)Cl phase is prominent, but some peaks at lower angles at 12.7 and 13.2° emerged and intensity of 32.5° declined (due to Cu(OH)Cl). The SM on further heating to 350° showed a drastic change with most of the peaks fitting into the Cu_2OCl_2 phase. Clear emergence of 17.6°, which is 100% peak of the Cu_2OCl_2 phase, was observed prominently in the temperature range of 350−450 °C. The low-angle peaks marked by $ as mentioned above suggested the copper chloride hydroxide hydrate $Cu_3Cl_4(OH)_2{\cdot}2H_2O$ phase. Continuous heating of SM helped in providing strong evidence of formation of the Cu_2OCl_2 phase *in situ* from CuO + $CuCl_2{\cdot}2H_2O$ *via* Cu(OH)Cl. As compared to repeated heating (Section 3.3.1), the presence of Cu_2OCl_2 is prominently noticeable in continuous heating mode during the temperature range of 350−450 °C. Our supposition mentioned above that $Cu_3Cl_4(OH)_2{\cdot}2H_2O$ is rendered due to the hygroscopic nature of Cu_2OCl_2 is probably true. As shown here, cooling was avoided, which helped in keeping the Cu_2OCl_2 phase intact and dominated over the hydrate phase. Furthermore, at 500 and 550 °C, formation and growth of the CuCl phase are observed. The continuous heating also helped in confirming that CuCl is formed at the expense or decomposition of the Cu_2OCl_2 phase. Thus, the continuous heating experiment without allowing cooling of the sample at every temperature provided enhanced insights about the intermediates formed at different temperatures during thermal decomposition of the SM.

3.4. *In Situ* XAS Studies. *In situ* XAS studies on the simulated feed and SM sample were performed in the temperature range of RT to 500 °C at BL-09, INDUS-2, RRCAT, Indore. XANES data of standard $CuCl_2$, CuCl, CuO, Cu_2OCl_2, and Cu metal were recorded for comparison as shown in Figure 5. Compounds with Cu(II) ions characteristically show three peaks; one is vibronically activated 1s to 3d transition that appears as a pre-edge at 8977 eV. Another is due to the forbidden transition from 1s to 4s, which appears as a shoulder at 8987 eV. The last is the allowed highest energy transition from 1s to 4p at 8997 eV, which finally merges with the continuum. However, spectra for +1 compounds, such as CuCl, with the d_{10} system are quite different. It lacks the pre-edge peak due to the absence of 1s to 3d transition, while a

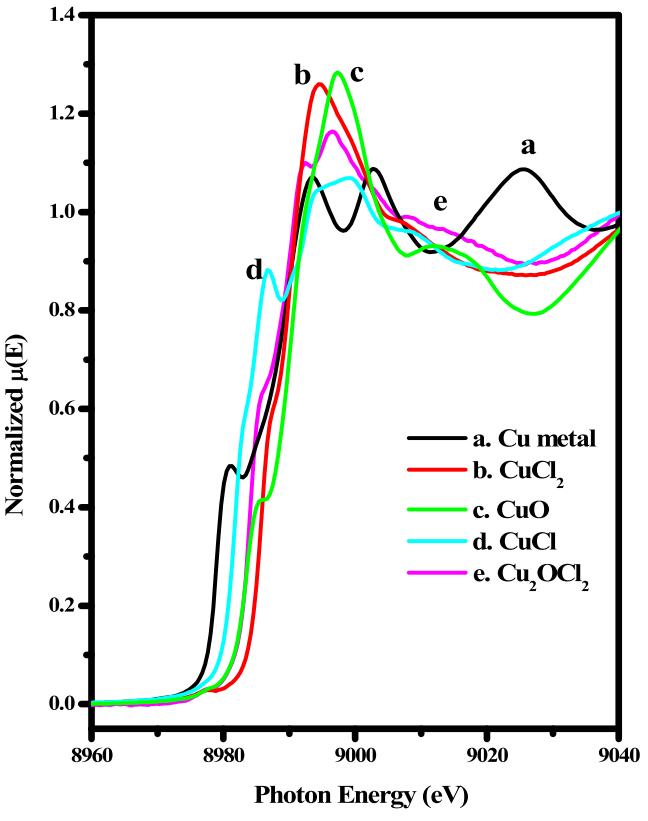


Figure 5. XANES spectra of the standard samples and (a) Cu metal, (b) $CuCl_2$, (c) CuO, (d) CuCl, and (e) Cu_2OCl_2 at the Cu K edge.

Downloaded from pubs.acs.org/enfuem/article-pdf/37/19/15206/12589762/ef3c02035.pdf by DOKUZ EYLUL UNIV user on 31 August 2026

https://doi.org/10.1021/acs.energyfuels.3c02035
Energy Fuels 2023, 37, 15206−15221

sharp peak observed at 8987 eV is attributed to 1s to 4s transition. Thus, the absence of the pre-edge peak and a sharp transition peak at 8987 are characteristic of Cu(I) compounds.[33,34]

After standards, *in situ* XANES spectra were recorded for SM (1:1 $CuCl_2$ + CuO mixture) in the temperature range of RT to 500 °C with an increase of 50 °C (Figure 6). For this purpose,

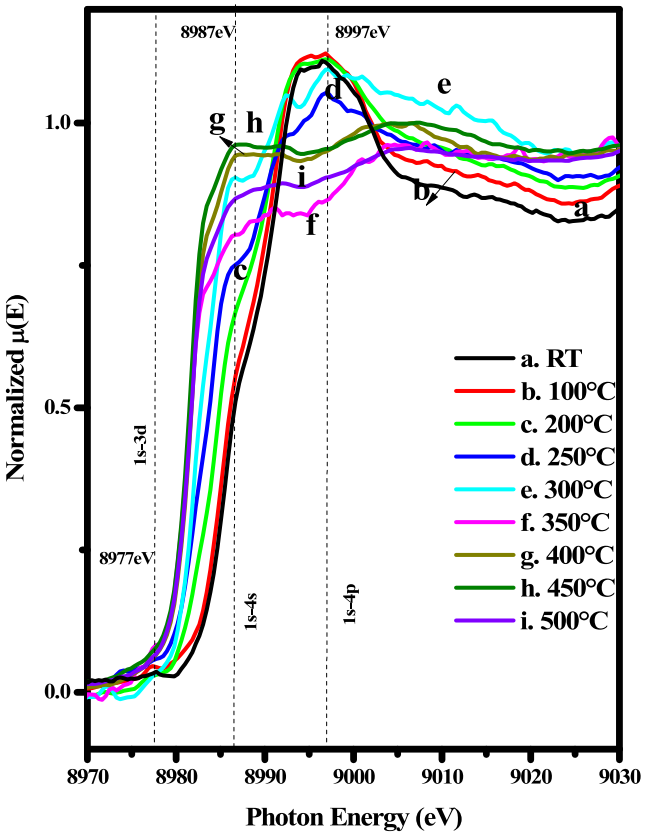


Figure 6. *In situ* XANES spectra recorded at the Cu K edge during the thermal decomposition of SM under an argon flow at various temperatures in the range of RT to 500 °C.

the sample was kept and heated in a capillary tube quartz reactor as shown in Figure 2. XANES spectra at RT have features of Cu(II) species with a pre-edge peak at 8977 eV (1s → 3d) and a shoulder at 8987 eV (1s → 4s) and peak at 8997 eV (1s → 4p), which is understood due to the presence of Cu(II) species $CuCl_2$ and CuO (Figure 6). Spectra at 300 °C had a clear pre-edge, a shoulder, and a peak in the range of 8990−9005 eV that matched with features due to standard Cu_2OCl_2, confirming the *in situ* formation of Cu_2OCl_2. XANES spectra in e and f curves corresponding to 300 and 350 °C are similar, indicating the presence of the Cu_2OCl_2 phase. On further heating the sample above 400 °C, the absorption edge shifts toward lower energy with an increase in temperature. This is evidence of formation of CuCl. At 500 °C, XANES spectra match completely with those of the standard CuCl, pointing out that CuCl is the only species present above 500 °C. The % composition of different phases during the course of heating was estimated by linear combination fitting (LCF) of XANES data. Starting materials $CuCl_2$ and CuO (1:1 molar mixture) were estimated to be 58−65 and 42−35 wt %, respectively, in the range of RT to 200 °C. With the increase in temperature beyond 200 °C, formation of Cu_2OCl_2 was evident; at an onset temperature of 300 °C, its contribution increased up to 350 °C and declined at temperatures beyond 400 °C. The CuCl phase appeared at 300 °C and increased with an increase in temperature at the expense of Cu_2OCl_2 and starting materials. The CuCl concentration was 100% at 500 °C.

EXAFS oscillations have been extracted from the X ray absorption spectra $\mu(E)$ *versus* E, following the standard procedure.[35,36] The EXAFS oscillation $\chi(k)$ is weighted by k^2 to amplify the oscillation at high k and the functions $\chi(k)\ k^2$ are Fourier-transformed using a k range of 2−8 $Å^{-1}$ to generate the $\chi(r)$ *versus* r (or FT-EXAFS) spectra in terms of the real distances from the center of the absorbing atom. It should be mentioned here that a set of EXAFS data analysis programs available within the Demeter software package have been used for reduction and fitting of the experimental EXAFS data. This includes data reduction and Fourier transform to derive the $\chi(r)$ *versus* r plots from the absorption spectra, generation of the theoretical EXAFS spectra starting from an assumed crystallographic structure, and finally fitting of the experimental $\chi(r)$ *versus* r data with the theoretical ones using the FEFF 6.0 code.

Figure 7 shows the $\chi(r)$ *versus* r plots recorded during the thermolysis of the CuO and $CuCl_2$ mixture sample. The

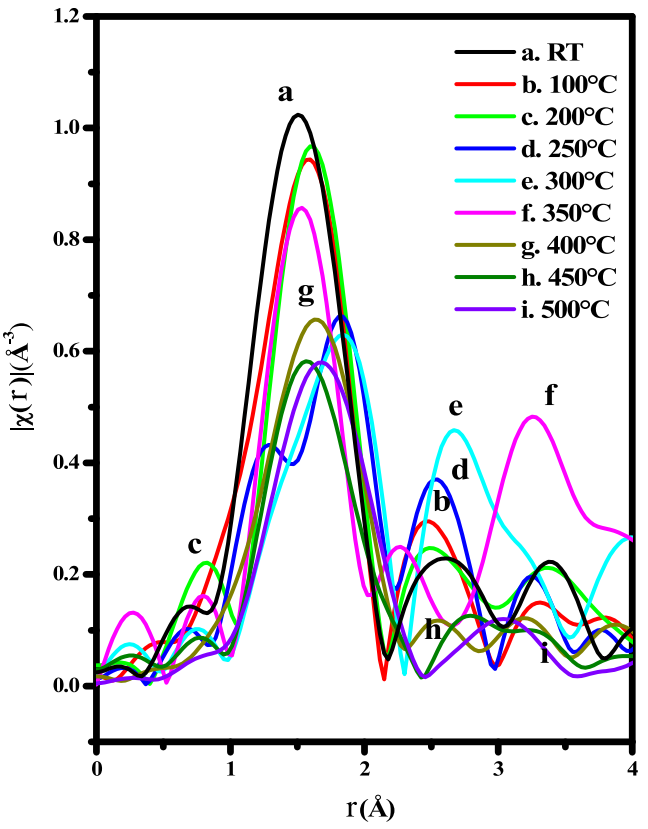


Figure 7. $\chi(r)$ *versus* r plots recorded during the thermal decomposition of SM under an argon flow at various temperatures in the range of RT to 500°C.

experimental $\chi(r)$ *versus* r data have been fitted from 1 to 3 Å, assuming a Cu−O shell at 1.944 Å, a Cu−Cl shell at 2.284 Å, and a Cu−Cu shell at 3.050 Å. The coordination number, bond distance, and disorder (Debye−Waller) factors (σ^2), which give the mean-square fluctuations in the distances, have

Downloaded from pubs.acs.org/enfuem/article-pdf/37/19/15206/12589762/ef3c02035.pdf by DOKUZ EYLUL UNIV user on 31 August 2026

https://doi.org/10.1021/acs.energyfuels.3c02035
Energy Fuels 2023, 37, 15206−15221

been used as fitting parameters. The EXAFS fitting results for the sample along with that of standards are tabulated in Table 4. Cu cations in the Cu_2OCl_2 structure are surrounded by two chlorine and three oxygen ions at distances of 2.25 and 1.94 Å, respectively,[15] while in the CuO structure, four oxygen ions surround Cu cations at a distance of 1.94 Å.[37,3837,38] Both Cu_2OCl_2 and CuO have a Cu−Cu distance of around 2.95 Å.

From Table 4, it is evident that at room temperature, the Cu−Cl and CuO bond distances 2.35 and 1.94 Å, respectively, are in close agreement with bond distances of standard $CuCl_2$ and CuO. Also, since we have analyzed a mixture of $CuCl_2$ and CuO phases, the coordination numbers are not in close agreement as there will be interferences in the measurement. As the temperature increases up to 350 °C, Cu−O, Cu−Cl, and Cu−Cu bond distances approach toward the Cu_2OCl_2, confirming formation of the Cu_2OCl_2 phase around 350 °C. After 400 °C, the Cu−Cl bond distance and coordination number approach 2.25 Å and 3, respectively. At 500 °C, the bond distances and coordination number are a close match to those of CuCl, confirming the formation of the CuCl phase.

4. DISCUSSION

The above-mentioned TG-MS studies investigated the oxygen evolution behavior of actual hydrolysis products and compared it with the simulated pure and impure feeds. These studies provided valuable information about the variation in the onset temperature of oxygen with the presence or absence of the impurity phase. Also, it helped in establishing and validating the methodology of quantification of the Cu_2OCl_2 phase when subjected to TG and resulted in the O_2 evolution peak at 400−500 °C. By comparing the observed weight loss with the expected one, various inferences were drawn particularly in impure simulated feeds. The observed weight loss for O_2 evolution from impure feeds was lower than that of the SM. One of the main inferences drawn was that O_2 evolution in impure feeds can be predetermined. Irrespective of the kind of impurity, it is governed by the maximum number of notional Cu_2OCl_2 moles possible in the impure composition. The O_2 evolution methodology also helped in suggesting the purity of the Cu_2OCl_2 phase formed during the hydrolysis step as shown in Table 5. Another important result was that the simulated feed, SM (equimolar mixture of CuO and $CuCl_2$), behaved almost identical to the actual hydrolysis product with more than 95% purity in terms of the O_2 evolution and thermal decomposition profile. Furthermore, to understand how the two behave similarly, the mechanism involved in thermal decomposition of the SM was investigated using *ex situ* HTXRD studies and *in situ* XAS. The intermediate phases formed at various temperatures when the SM was subjected to heat treatment under an argon flow from RT to 550 °C were identified by XRD. As explained in Section 3.3, the SM was subjected to heat treatment by adopting two different methodologies, *viz.*, continuous heating without cooling (Figure 4a), and the other was repeated heating followed by cooling cycles (Figure 4b). It provided evidence of the following: (i) The CuO + $CuCl_2{\cdot}2H_2O$ mixture on heating at 100−150 °C forms single phase Cu(OH)Cl, which strengthens up to 250 °C. (ii) Strong peaks due to formation of Cu_2OCl_2 from Cu(OH)Cl in the temperature range of 350−450 °C was observed. The onset temperature in continuous heating was at 350 °C, higher as compared to 300 °C observed in repeated heating temperature programming. The system during repeated heating probably achieves thermal equilibrium,

Table 4. Bond Length (r), Coordination Number (N), and Disorder Factor (σ^2) Derived from EXAFS Recorded during Heating of the Simulated Mixture (SM) at Different Temperatures at the Cu K-Edge

	Cu−O			Cu−Cl			Cu−Cu		
temperature	r (Å)	N	σ^2 (Å^2)	r (Å)	N	σ^2 (Å^2)	r (Å)	N	σ^2 (Å^2)
RT	1.94 ± 0.01	2.7 ± 0.2	0.0027 ± 0.0016	2.35 ± 0.03	1.9 ± 0.3	0.0187 ± 0.0119	3.07 ± 0.04	5.8 ± 0.2	0.0112 ± 0.0083
100 °C	2.00 ± 0.03	2.7 ± 0.5	0.0120 ± 0.0035	2.26 ± 0.04	2.9 ± 0.5	0.0227 ± 0.0136	3.09 ± 0.05	5.8 ± 0.5	0.0097 ± 0.0069
200 °C	2.04 ± 0.01	2.5 ± 0.2	0.0010 ± 0.0009	2.20 ± 0.03	2.6 ± 0.3	0.0219 ± 0.0041	3.07 ± 0.05	5.4 ± 0.2	0.0119 ± 0.0058
250 °C	1.98 ± 0.01	1.8 ± 0.1	0.0109 ± 0.0037	2.33 ± 0.01	2.6 ± 0.2	0.0246 ± 0.0041	3.01 ± 0.02	3.7 ± 0.1	0.0156 ± 0.0032
300 °C	2.00 ± 0.03	2.3 ± 0.3	0.0127 ± 0.0114	2.32 ± 0.03	2.7 ± 0.4	0.0249 ± 0.0092	3.01 ± 0.03	4.6 ± 0.3	0.0146 ± 0.0054
350 °C	1.91 ± 0.02	2.3 ± 0.3	0.0127 ± 0.0046	2.32 ± 0.02	2.4 ± 0.3	0.0249 ± 0.0198	3.01 ± 0.03	4.6 ± 0.3	0.0146 ± 0.0077
400 °C				2.21 ± 0.02	2.8 ± 0.2	0.0129 ± 0.0064			
450 °C				2.20 ± 0.04	2.6 ± 0.3	0.0134 ± 0.0083			
500 °C				2.27 ± 0.05	2.9 ± 0.3	0.0151 ± 0.0094			
$CuCl_2$				2.25 ± 0.04	3.99 ± 0.25	0.0059 ± 0.0010			
CuO	1.94 ± 0.02	3.8 ± 0.3	0.0046 ± 0.0012				2.95 ± 0.02	5.4 ± 0.3	0.0261 ± 0.0048
Cu_2OCl_2	1.94 ± 0.01	2.91 ± 0.18	0.0035 ± 0.009	2.25 ± 0.01	1.94 ± 0.12	0.0102 ± 0.0013	2.94 ± 0.01	3.88 ± 0.24	0.0220 ± 0.0009
CuCl				2.26 ± 0.02	3.05 ± 0.10	0.0106 ± 0.0013			

Downloaded from pubs.acs.org/enfuem/article-pdf/37/19/15206/12589762/ef3c02035.pdf by DOKUZ EYLUL UNIV user on 31 August 2026

https://doi.org/10.1021/acs.energyfuels.3c02035
Energy Fuels 2023, 37, 15206−15221

Table 5. O_2 Evolved by Thermal Degradation of Hydrolysis Products and Simulated Feeds during the Decomposition Step Evaluated by TG-MS

sample	% observed wt loss due to O_2 evolved in 400−530 °C	expected % wt loss due to O_2 evolution in 400−530 °C	% purity based on O_2 evolution at low temperature[a]
HP-Fix-1	7.07	7.47	94.6
HP-Fix-2	5.97	7.47	79.9
HP-Flu-1	7.15	7.47	95.7
HP-Flu-2	3.67	7.47	67.7
SM	7.24	7.47	96.9
IMP-1	5.04	7.47	67.4
IMP-2	4.32	7.47	57.8

[a]Calculated considering weight loss due to the reaction at 350−500 °C: $CuCl_2{\cdot}CuO \rightarrow 2CuCl + 0.5O_2$. % purity = 100 × observed weight loss/expected weight loss.

while during continuous heating, enough time was not given to the system to achieve thermal equilibrium. Thus, anomaly of 50 °C was observed. (iii) At 400 °C, formation of small amounts of the copper chloride hydroxide hydrate $Cu_3Cl_4(OH)_2{\cdot}2H_2O$ phase along with the Cu_2OCl_2 phase is indicated. This can be considered a transition phase in which hydrate melt is formed and it undergoes decomposition to CuCl. (iv) Lastly, Cu_2OCl_2 which existed up to 450 °C decomposes to CuCl along with evolution of O_2. Growth of single phase CuCl was observed up to 550 °C. Thus, a probable pathway for thermal decomposition of SM can be written as in Table 6.

Other researchers have studied the decomposition step using either copper oxychloride, Cu_2OCl_2, or an equimolar mixture of $CuCl_2$ and CuO. One of the mechanistic approaches reported by Serban et al. in 2004[39] is shown by eqs 16 and 17. In this, after performing the decomposition step, using an equimolar mixture of CuO and $CuCl_2$, it was concluded that oxygen evolution is limited by the decomposition of $CuCl_2$ (eq 16). According to that report, the presence of CuO helps in two ways: first, it promotes the release of Cl_2 (eq 16), and second, it helps in complete consumption of Cl_2 released (eq 17), giving out CuCl with evolution of O_2 as the only decomposition product.

$$CuCl_2(s) \rightarrow CuCl(s) + 0.5Cl_2(g) \quad (16)$$

$$CuO(s) + 0.5Cl_2(g) \rightarrow CuCl(s) + 0.5O_2(g) \quad (17)$$

Our studies add to Serban's approach by stating that the presence of CuO helps in abstraction of Cl_2 *via* formation of copper hydroxy chloride first (CuOHCl) and later copper oxychloride as intermediates and further dissociate into O_2 and CuCl. Our earlier study[16] has shown Cl_2 evolution from $CuCl_2$ alone; however, in the present study, evolution of Cl_2 is not observed in MS from the CuO + $CuCl_2$ mixture. The absence of Cl_2 evolution during decomposition of SM indicates that CuO abstracts Cl_2 and forms an intermediate compound, Cu_2OCl_2. This also explains the identical thermal behavior of the equimolar mixture of CuO and $CuCl_2$, SM, and actual hydrolysis product. Thus, all the above-mentioned discussion further strengthens the supposition that an equimolar mixture of CuO and $CuCl_2$ can substitute the hydrolysis product, Cu_2OCl_2. A cycle based on CuO + $CuCl_2$ as the feed for the decomposition step is already proposed by Thomas et al.[21] In this cycle, CuO is proposed to be the product in the hydrolysis step instead of Cu_2OCl_2 and the modified reactions involved in each step are shown below using eqs 18−21

$$\text{electrochemical step: } 2CuCl(aq) + 2HCl \rightarrow 2CuCl_2(aq) + H_2 \quad (18)$$

$$\text{drying step: } 2CuCl_2(aq) \rightarrow 2CuCl_2(s) \quad (19)$$

$$\text{hydrolysis step: } CuCl_2(s) + H_2O(g) \rightarrow CuO(s) + 2HCl \quad (20)$$

$$\text{decomposition step: } CuCl_2(s) + CuO(s) \rightarrow 2CuCl(s) + 0.5O_2 \quad (21)$$

As reported by Thomas et al.,[21] half moles of $CuCl_2$ produced in the electrochemical step will be used as the feed for the hydrolysis step and the other half will be used for the decomposition step. It has an advantage that it avoids Cu_2OCl_2 as the intermediate of the Cu−Cl cycle. Preparation of Cu_2OCl_2 requires critical experimental conditions as compared to stable CuO. Dealing with CuO is beneficial as it is non-hygroscopic and stable, while Cu_2OCl_2 is highly hygroscopic and relatively unstable. As reported and discussed in the above-mentioned sections, formation of 100% phase-pure Cu_2OCl_2 is most unlikely. Due to the instability and labile nature of Cu_2OCl_2, it is mostly associated with impure phases such as CuCl, CuO, or $CuCl_2$. Thus, operation of the closed-loop Cu−Cl process at the engineering scale based on CuO + $CuCl_2$ as the feed for the decomposition step will be relieved from handling and storage issues of Cu_2OCl_2. However, the cycle using CuO + $CuCl_2$ as the modified feed for decomposition step may suffer from involvement of additional drying, grinding, and mixing of CuO and $CuCl_2$ prior to the decomposition step. A scaled-up process, for example, H_2 production targeted @5 m^3/h and corresponding stoichiometric O_2 production @2.5 m^3/h, will require 30.01 kg of

Table 6. A Pro Thermal Decomposition Pathway of SM (1:1 CuO + $CuCl_2$) Is Proposed along with Species Identified by XRD and MS

temperature (°C)	reaction proposed	phase identification by XRD	species identified by MS
RT	$CuCl_2{\cdot}2H_2O + CuO$	$CuCl_2{\cdot}2H_2O$, CuO, Cu(OH)Cl (minor)	none
100−250 °C	$CuCl_2{\cdot}2H_2O(s) + CuO(s) \rightarrow Cu(OH)Cl(s) + H_2O(g)$	Cu(OH)Cl	H_2O
300−350 °C	$2Cu(OH)Cl(s) \rightarrow Cu_2OCl_2(s) + H_2O(g)$	$Cu_2OCl_2(s)$ and hydrate phase	H_2O
400 °C	$3Cu_2OCl_2(s) + H_2O \rightarrow$ hydrate phase (such as $Cu_3Cl_4(OH)_2{\cdot}2H_2O$) + 2Cu(OH)Cl	$Cu_3Cl_4(OH)_2{\cdot}2H_2O$, Cu(OH)Cl, Cu_2OCl_2	none
450−550 °C	$Cu_2OCl_2(s) \rightarrow 2CuCl + O_2$	CuCl(s)	O_2
$T \geq 550$ °C	$CuCl(s) \rightarrow CuCl(g)$	CuCl(s)	evaporation of CuCl

https://doi.org/10.1021/acs.energyfuels.3c02035
Energy Fuels 2023, 37, 15206−15221

Downloaded from pubs.acs.org/enfuem/article-pdf/37/19/15206/12589762/ef3c02035.pdf by DOKUZ EYLUL UNIV user on 31 August 2026

$CuCl_2$ and 17.75 kg of CuO per hour as feed for the decomposition step. The strategy of drying, mixing, and grinding used for close contact between CuO and $CuCl_2$ phases will surely affect the overall energy and cost economics of the cycle. Thus, it will be desirable to look for alternative options such as precipitating $CuCl_2$ over CuO in a core−shell type fashion to achieve close contact. This will combine both drying and mixing in one step and will avoid grinding. The exact cost, economics, and detailed critical examination of using CuO + $CuCl_2$ as feed for the decomposition step and modifying the Cu−Cl cycle based on the modified feed are a subject beyond the scope of the present work.

The Cu−Cl cycle is dominated with copper compounds, particularly $CuCl_2$, CuCl, CuO, Cu_2OCl_2, and Cu(OH)Cl. Except CuO, all other compounds have poor stability. In both thermal steps—hydrolysis and decomposition—both starting and final products are chlorides/oxychlorides. However, CuO is also observed as a byproduct in both steps. Thus, due to the labile nature of Cu_2OCl_2[16] and unstable $CuCl_2$, a very complex chemistry occurs and the mixture of mixed phases is formed at different temperatures. A schematic in which all possible reactions/pathways that can be adopted by $CuCl_2$ in the presence of steam (hydrolysis) or absence of steam (thermolysis) is shown in Figure 8. $CuCl_2$ on heating in air

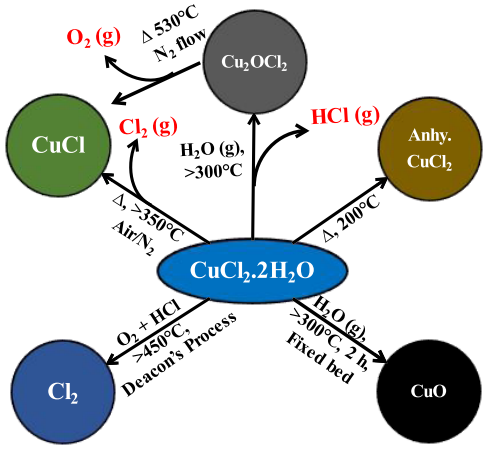


Figure 8. Schematic of possible reaction pathways which the reactant $CuCl_2$ can adopt when subjected to thermal treatment under different reaction conditions. One of the reaction conditions depicts the hydrolysis step of the Cu−Cl cycle in which Cu_2OCl_2 is formed. Prominent undesirable possibilities are parallel thermolysis of $CuCl_2$ to CuCl and Deacon's process in the presence of HCl at much high $T \geq 450$ °C.

first converts into anhydrous $CuCl_2$ in the temperature range of 100−200 °C. Furthermore, heating of anhy. $CuCl_2$ in air does not yield oxide; instead, due to its poor stability, it invariably undergoes thermolysis to CuCl accompanied with evolution of Cl_2. CuCl(s) is very different form $CuCl_2$ in physical and chemical properties as reported earlier.[16] In the presence of excess of steam, $CuCl_2$ gets hydrolyzed to Cu_2OCl_2 (hydrolysis step of the Cu−Cl cycle) in the temperature range of 300−400 °C along with evolution of HCl gas. However, hydrolysis if continued for a longer duration yields a single phase of CuO. Cu_2OCl_2 if heated in an inert atmosphere at $T \geq 350$ °C on further heating decomposes into CuO + $CuCl_2$. If the temperature exceeds more than 450 °C, then, the possibility of the Deacon's process increases. HCl gas is oxidized by atmospheric O_2 in the presence of $CuCl_2$ as a catalyst at 450 °C during Deacon's process. Instability of copper chlorides renders complexity in the thermal steps of the Cu−Cl cycle.

5. CONCLUSIONS

Here, in the present study, the role of the impurity phase associated with the hydrolysis product in decomposition kinetics was investigated using TG-MS. The thermal degradation pathway of actual hydrolysis products was investigated and compared with the simulated pure and impure feeds. Actual hydrolysis products were obtained by fixed-bed and fluidized-bed $CuCl_2$ hydrolysis. Simulated feeds consisted of (a) CuO + $CuCl_2$ in 1:1 molar ratio, known as the substitute material (SM) to Cu_2OCl_2, (b) 2CuO + $CuCl_2$ (Imp-1) having a known amount of CuO as the impurity phase, and (c) 2CuO + $CuCl_2$ + 0.5CuCl (Imp-2). The observed weight loss due to O_2 evolution in the thermogram of SM was close to that expected; also, it matched completely with the phase-pure actual hydrolysis product Cu_2OCl_2. Thus, TG-MS studies showed that the thermal behavior of the SM is identical to that of Cu_2OCl_2, while impure feeds when subjected to TG lowered the O_2 evolution temperature by 40 °C and yield by 50%. The observed weight loss was almost 50% lower than the expected weight loss irrespective of the kind of impurity. An explanation with the help of equations is given above, which showed that moles of O_2 evolved from impure samples is limited by x, where x is the maximum moles of Cu_2OCl_2 possible in the impure composition. The present study also revealed and confirmed the *in situ* formation of Cu_2OCl_2 *via* Cu(OH)Cl from the equimolar CuO + $CuCl_2$ (SM) mixture in the temperature range of 300−350 °C. Also, Cu_2OCl_2 formed further decomposes at $T \geq 500$ °C to form CuCl and O_2. At 400 °C along with Cu_2OCl_2, another minor phase of copper chloride hydroxide hydrate, $Cu_3Cl_4(OH)_2 \cdot 2H_2O$, was also present. The minor phase may be a result of the hygroscopic nature of Cu_2OCl_2. Above 400 °C, Cu_2OCl_2 transforms into CuCl and O_2. Our studies add to Serban's approach[39] and convey that abstraction of Cl_2 by CuO may be facilitated *via* Cu_2OCl_2 formation. This also explains the absence of the free Cl_2 peak in MS during thermal decomposition of the SM. For this, the variations in the local structure around Cu in SM were also investigated using the *in situ* XAS tool in the temperature range of RT to 500 °C. As the temperature increases up to 350 °C, Cu−O, Cu−Cl, and Cu−Cu bond distances approach that of the Cu_2OCl_2, confirming the formation of the Cu_2OCl_2 phase. After 400 °C, the Cu−Cl bond distance and coordination number approach 2.25 Å and 3, respectively. At 500 °C, the bond distances and coordination number are a close match to that of CuCl, confirming the formation of the CuCl phase. Phase compositions at intermediate temperatures were also monitored using continuous and repeated heating modes of *ex situ* HT-XRD. Both studies confirmed and established our proposition that an equimolar mixture of CuO + $CuCl_2$ (SM) can be an ideal substitute for Cu_2OCl_2 (which is commercially unavailable) required for studies on the Cu−Cl cycle. The results from the above-mentioned studies will be useful for large-scale closed-loop operation of the Cu−Cl process.

Downloaded from pubs.acs.org/enfuem/article-pdf/37/19/15206/12589762/ef3c02035.pdf by DOKUZ EYLUL UNIV user on 31 August 2026

https://doi.org/10.1021/acs.energyfuels.3c02035
Energy Fuels 2023, 37, 15206−15221

■ ASSOCIATED CONTENT

Supporting Information

The Supporting Information is available free of charge at https://pubs.acs.org/doi/10.1021/acs.energyfuels.3c02035.

Experimental details of fixed-bed and fluidized-bed $CuCl_2$ hydrolysis, schematic of the fixed-bed reactor, calibration of TG-MS, and XRD of the starting compounds (PDF)

■ AUTHOR INFORMATION

Corresponding Author

Mrinal R. Pai − *Chemistry Division, Bhabha Atomic Research Centre, Mumbai 400085 Maharashtra, India; Homi Bhabha National Institute, Mumbai 400085 Maharashtra, India;* orcid.org/0000-0002-5243-7971; Phone: 91 22 25592288; Email: mrinalr@barc.gov.in, mrinalpai9@gmail.com; Fax: 9122 25505151

Authors

Rajendra V. Singh − *Chemistry Division, Bhabha Atomic Research Centre, Mumbai 400085 Maharashtra, India; Homi Bhabha National Institute, Mumbai 400085 Maharashtra, India*

Atindra M. Banerjee − *Chemistry Division, Bhabha Atomic Research Centre, Mumbai 400085 Maharashtra, India; Homi Bhabha National Institute, Mumbai 400085 Maharashtra, India*

Deepa Thomas − *Chemical Engineering Division, Bhabha Atomic Research Centre, Mumbai 400085 Maharashtra, India; Homi Bhabha National Institute, Mumbai 400085 Maharashtra, India;* orcid.org/0000-0002-2241-8104

Geeta S. Patkare − *Fuel Chemistry Division, Bhabha Atomic Research Centre, Mumbai 400085 Maharashtra, India*

Suhas Phapale − *Chemistry Division, Bhabha Atomic Research Centre, Mumbai 400085 Maharashtra, India*

Chandrani Nayak − *Atomic & Molecular Physics Division, Bhabha Atomic Research Centre, Mumbai 400085 Maharashtra, India*

Vidha Bhasin − *Atomic & Molecular Physics Division, Bhabha Atomic Research Centre, Mumbai 400085 Maharashtra, India; Homi Bhabha National Institute, Mumbai 400085 Maharashtra, India*

Arvind K. Tripathi − *Chemistry Division, Bhabha Atomic Research Centre, Mumbai 400085 Maharashtra, India; Homi Bhabha National Institute, Mumbai 400085 Maharashtra, India*

Complete contact information is available at: https://pubs.acs.org/10.1021/acs.energyfuels.3c02035

Notes

The authors declare no competing financial interest.

■ ACKNOWLEDGMENTS

The authors thank D. Bhattacharyya, Atomic & Molecular Physics Division, BARC, for XAS experiments. The authors thank Dr. A. K. Tyagi, Director, Chemistry Group, BARC, Dr. S. Mukhopadhyay, Head Chemical Engineering Division, and Dr. K. T. Shenoy, Director, Chemical Engineering Group, for their kind support and encouragement.

■ REFERENCES

(1) Dutta, S. Review on Solar Hydrogen: Its Prospects and Limitations. *Energy Fuels* **2021**, *35*, 11613−11639.

(2) Song, H.; Luo, S.; Huang, H.; Deng, B.; Ye, J. Solar-Driven Hydrogen Production: Recent Advances, Challenges, and Future Perspectives. *ACS Energy Lett.* **2022**, *7*, 1043−1065.

(3) Mehrpooya, M.; Habibi, R. A review on hydrogen production thermochemical water-splitting cycles. *J. Cleaner Prod.* **2020**, *275*, No. 123836.

(4) Razi, F.; Dincer, I. A critical evaluation of potential routes of solar hydrogen production for sustainable development. *J. Cleaner Prod.* **2020**, *264*, No. 121582.

(5) Boretti, A. Concentrated Solar Energy with Thermal Energy Storage for Hydrogen Production by Three-Step Thermochemical Water-Splitting Cycles. *Energy Fuels* **2021**, *35*, 10832−10840.

(6) Kodama, T.; Gokon, N. Thermochemical Cycles for High-Temperature Solar Hydrogen Production. *Chem. Rev.* **2007**, *107*, 4048−4077.

(7) Safari, F.; Dincer, I. A review and comparative evaluation of thermochemical water splitting cycles for hydrogen production. *Energy Convers. Manage.* **2020**, *205*, No. 112182.

(8) Dulera, I. V.; Sinha, R. K. High temperature reactors. *J. Nucl. Mater.* **2008**, *383*, 183−188.

(9) Wang, Z.; Naterer, G. F.; Gabriel, K. S.; Secnik, E.; Gravelsins, R.; Daggupati, V. Thermal design of a solar hydrogen plant with a copper−chlorine cycle and molten salt energy storage. *Int. J. Hydrogen Energy* **2011**, *36*, 11258−11272.

(10) Chakrabarty, D. K. *An Introduction to Physical Chemistry*; Alpha Science International Ltd.: Mumbai, 2001.

(11) Kubo, S.; Nakajima, H.; Kasahara, S.; Higashi, S.; Masaki, T.; Abe, H.; Onuki, K. A demonstration study on a closed-cycle hydrogen production by the thermochemical water-splitting iodine−sulfur process. *Nucl. Eng. Des.* **2004**, *233*, 347−354.

(12) Nadar, A.; Banerjee, A. M.; Pai, M. R.; Meena, S. S.; Patra, A. K.; Sastry, P. U.; Singh, R.; Singh, M. K.; Tripathi, A. K. Immobilization of crystalline Fe_2O_3 nanoparticles over SiO_2 for creating an active and stable catalyst: A demand for high temperature sulfuric acid decomposition. *Appl. Catal.* **2021**, *283*, No. 119610.

(13) Nadar, A.; Banerjee, A. M.; Pai, M. R.; Meena, S. S.; Pai, R. V.; Tewari, R.; Yusuf, S. M.; Tripathi, A. K.; Bharadwaj, S. R. Nanostructured Fe_2O_3 dispersed on SiO_2 as catalyst for high temperature sulfuric acid decomposition—Structural and morphological modifications on catalytic use and relevance of Fe_2O_3-SiO_2 interactions. *Appl. Catal.* **2017**, *217*, 154−168.

(14) Banerjee, A. M.; Pai, M. R.; Tewari, R.; Raje, N.; Tripathi, A. K.; Bharadwaj, S. R.; Das, D. A Comprehensive Study on Pt/Al_2O_3 Granular Catalyst used for Sulfuric Acid Decomposition Step in Sulfur-Iodine Thermochemical Cycle: Changes in Catalyst Structure, Morphology and Metal-Support Interaction. *Appl. Catal.* **2015**, *162*, 327−337.

(15) Singh, R. V.; Pai, M. R.; Banerjee, A. M.; Nayak, C.; Phapale, S.; Bhattacharyya, D.; Tripathi, A. K. Cu-Cl Thermochemical Water Splitting Cycle: Probing Temperature Dependent $CuCl_2$ Hydrolysis and Thermolysis Reaction using *in-situ* XAS. *J. Therm. Anal. Calorim.* **2022**, *147*, 7063−7076.

(16) Singh, R. V.; Pai, M. R.; Banerjee, A. M.; Patkare, G. R.; Pai, R. V.; Kumar, A.; Yadav, A. K.; Phaphale, S.; Tripathi, A. K. Investigations on the hydrolysis step of copper-chlorine thermochemical cycle for hydrogen production. *Int. J. Energy Res.* **2020**, *44*, 2845−2863.

(17) Banerjee, A. M.; Antony, R. P.; Pai, M. R.; Kumar, A.; Tripathi, A. K. Investigations on a platinum catalyzed membrane for electrolysis step of copper-chlorine thermochemical cycle for hydrogen production. *Int. J. Energy Res.* **2021**, *45*, 5912−5921.

(18) Farsi, A.; Dincer, I.; Naterer, G. F. Review and evaluation of clean hydrogen production by the copper−chlorine thermochemical cycle. *J. Cleaner Prod.* **2020**, *276*, No. 123833.

(19) Li, H.; Stolberg, L.; Vega, A.; Zhang, W.; Reinwald, S.; Ryland, D.; Boniface, H.; Suppiah, S. Canadian advances in the copper−

Downloaded from pubs.acs.org/enfuem/article-pdf/37/19/15206/12589762/ef3c02035.pdf by DOKUZ EYLUL UNIV user on 31 August 2026

chlorine thermochemical cycle for clean hydrogen production: A focus on electrolysis. *Int. J. Hydrogen Energy* **2020**, *45*, 33037−33046.
(20) Orhan, M. F.; Dincer, I.; Rosen, M. A. The oxygen production step of a copper−chlorine thermochemical water decomposition cycle for hydrogen production: Energy and exergy analyses. *Chem. Eng. Sci.* **2009**, *64*, 860−869.
(21) Thomas, D.; Baveja, N. A.; Shenoy, K. T.; Joshi, J. B. Mechanistic and kinetic study of thermolysis reaction with hydrolysis step products in Cu−Cl thermochemical cycle. *Int. J. Hydrogen Energy* **2021**, *46*, 12672−12681.
(22) Krivovichev, S. V.; Filatov, S. K.; Burns, P. C. The cuprite-like framework of OCu_4 tetrahedra in the crystal structure of synthetic melanothallite, Cu_2OCl_2, and its negative thermal expansion. *Can. Mineral.* **2002**, *40*, 1185−1190.
(23) Kawashima, K.; Okabe, H.; Suzuki, K.; Kuroiwa, S.; Akimitsu, J.; Sato, K. H.; Koda, A.; Kadono, R. Antiferromagnetic ordering in Cu_2OCl_2 studied by the muon spin rotation/relaxation technique. *J. Phys.: Condens. Matter* **2007**, *19*, No. 145275.
(24) Nixon, A.; Ferrandon, M.; Kaye, M. H.; Trevani, L. Thermochemical production of hydrogen: Synthesis, characterization, and decomposition of copper oxychloride. *J. Therm. Anal. Calorim.* **2012**, *110*, 1095−1105.
(25) Thomas, D.; Baveja, N. A.; Shenoy, K. T.; Joshi, J. B. Experimental Study on the Mechanism and Kinetics of $CuCl_2$ Hydrolysis Reaction of the Cu−Cl Thermochemical Cycle in a Fluidized Bed Reactor. *Ind. Eng. Chem. Res.* **2020**, *59*, 12028−12037.
(26) Ferrandon, M. S.; Lewis, M. A.; Alvarez, F.; Shafirovich, E. Hydrolysis of $CuCl_2$ in Cu-Cl thermochemical cycle for hydrogen production: Experimental studies using a spray reactor with an ultrasonic atomizer. *Int. J. Hydrogen Energy* **2010**, *35*, 1895−1904.
(27) Lewis, M. A.; Masin, J. G.; Vilim, R. B. In *Development of the Low Temperature Cu-Cl Thermochemical Cycle*, International Congress on Advances in Nuclear Power Plants, May 15−19, Seoul, Korea, 2005.
(28) Marin, G. D.; Wang, Z.; Naterer, G. F.; Gabriel, K. Byproducts and reaction pathways for integration of the Cu-Cl cycle of hydrogen production. *Int. J. Hydrogen Energy* **2011**, *36*, 13414−13424.
(29) Dokiya, M.; Kotera, Y. Hybrid cycle with electrolysis using Cu-Cl system. *Int. J. Hydrogen Energy* **1976**, *1*, 117−121.
(30) Walter-Levy, M. L.; Goreaud, M. *Sur la Formation des Chlorures Culvriques par Vola Seche. II.—Thermolyse des Chlorures Neutras et Basiques*; Laboratorie de Chimie Minerale de la Faculte des Sciences de Caen, 1971.
(31) Poswal, A. K.; Agrawal, A.; Yadav, A. K.; Nayak, C.; Basu, S.; Kane, S. R.; Garg, C. K.; Bhattachryya, D.; Jha, S. N.; Sahoo, N. K. Commissioning and first results of scanning type EXAFS beamline (BL-09) at INDUS-2 synchrotron source. *AIP Conf. Proc.* **2014**, *1591*, 649−651.
(32) Basu, S.; Nayak, C.; Yadav, A. K.; Agrawal, A.; Poswal, A. K.; Bhattacharyya, D.; Jha, S. N.; Sahoo, N. K. A comparative facility for EXAFS measurements at INDUS-2 synchrotron source at RRCAT, Indore, India. *J. Phys.: Conf. Ser.* **2014**, *493*, No. 012032.
(33) Sarode, P. R.; Sankar, G.; Rao, C. N. R. XANES and EXAFS of copper compounds: studies of copper carboxylates with metal-metal bonds and of the complex formed by *Pseudomonas aeruginosa*. *Proc. Indian Acad. Sci.* **1983**, *92*, 527−542.
(34) Shulman, G. R.; Yafet, Y.; Eisenberger, P.; Blumberg, W. E. Observations and interpretation of X-ray absorption edges in iron compounds and proteins. *Proc. Natl. Acad. Sci. U.S.A.* **1976**, *73*, 1384−1388.
(35) Bunker, G. *Introduction to XAFS: A Practical Guide to X-ray Absorption Fine Structure Spectroscopy*; Cambridge University Press: Cambridge, 2010.
(36) Kelly, S. D.; Hesterberg, D.; Ravel, B.Analysis of Soils and Minerals Using X-ray Absorption Spectroscopy. In *Methods of Soil Analysis Part 5—Mineralogical Methods*; American Society of Agronomy, Crop Science Society of America, and Soil Science Society of America, 2008; Vol. *5*, pp 387−463.
(37) Ravel, B.; Newville, M. ATHENA, ARTEMIS, HEPHAESTUS: data analysis for X-ray absorption spectroscopy using IFEFFIT. *J. Synchrotron Radiat.* **2005**, *12*, 537−541.
(38) Ahmed, A.; Elvati, P.; Violi, A. Size and phase-dependent structure of copper (II) oxide nanoparticles. *RSC Adv.* **2015**, *5*, 35033−35041.
(39) Serban, M.; Lewis, M. A.; Basco, J. K. In *Kinetic Study of the Hydrogen and Oxygen Production Reactions in the Copper-Chlorine Thermochemical Cycle*, AIChe 2004 Spring National Meeting, April 25−29, 2004, New Orleans, LA, 2004.

Downloaded from pubs.acs.org/enfuem/article-pdf/37/19/15206/12589762/ef3c02035.pdf by DOKUZ EYLUL UNIV user on 31 August 2026

https://doi.org/10.1021/acs.energyfuels.3c02035
Energy Fuels 2023, 37, 15206−15221